Calpain mediates pulmonary vascular remodeling in rodent models of pulmonary hypertension, and its inhibition attenuates pathologic features of disease

Wanli Ma,[1] Weihong Han,[1] Peter A. Greer,[2] Rubin M. Tuder,[3] Haroldo A. Toque,[1] Kevin K.W. Wang,[4] R. William Caldwell,[1] and Yunchao Su[1,5,6,7]

[1]Department of Pharmacology and Toxicology, Medical College of Georgia, Georgia Health Sciences University, Augusta, Georgia, USA. [2]Queen's University Cancer Research Institute, Kingston, Ontario, Canada. [3]Department of Medicine, University of Colorado, Aurora, Colorado, USA. [4]Center of Innovative Research, Banyan Biomarkers Inc., Alachua, Florida, USA. [5]Department of Medicine, [6]Vascular Biology Center, and [7]Center for Biotechnology and Genomic Medicine, Medical College of Georgia, Georgia Health Sciences University, Augusta, Georgia, USA.

Pulmonary hypertension is a severe and progressive disease, a key feature of which is pulmonary vascular remodeling. Several growth factors, including EGF, PDGF, and TGF-β1, are involved in pulmonary vascular remodeling during pulmonary hypertension. However, increased knowledge of the downstream signaling cascades is needed if effective clinical interventions are to be developed. In this context, calpain provides an interesting candidate therapeutic target, since it is activated by EGF and PDGF and has been reported to activate TGF-β1. Thus, in this study, we examined the role of calpain in pulmonary vascular remodeling in two rodent models of pulmonary hypertension. These data showed that attenuated calpain activity in calpain-knockout mice or rats treated with a calpain inhibitor resulted in prevention of increased right ventricular systolic pressure, right ventricular hypertrophy, as well as collagen deposition and thickening of pulmonary arterioles in models of hypoxia- and monocrotaline-induced pulmonary hypertension. Additionally, inhibition of calpain in vitro blocked intracellular activation of TGF-β1, which led to attenuated Smad2/3 phosphorylation and collagen synthesis. Finally, smooth muscle cells of pulmonary arterioles from patients with pulmonary arterial hypertension showed higher levels of calpain activation and intracellular active TGF-β. Our data provide evidence that calpain mediates EGF- and PDGF-induced collagen synthesis and proliferation of pulmonary artery smooth muscle cells via an intracrine TGF-β1 pathway in pulmonary hypertension.

Introduction

Pulmonary hypertension is a severe and progressive disease characterized by increased pulmonary vascular resistance leading to right heart failure and death (1–3). Pulmonary vascular remodeling is an important common pathological feature of all categories of pulmonary hypertension. Accumulation of extracellular matrix, including collagen, and vascular smooth muscle cell proliferation and hypertrophy contribute to medial hypertrophy and muscularization, leading to obliteration of precapillary pulmonary arteries and sustained elevation of pulmonary arterial pressure (3, 4).

Several growth factors, including EGF, PDGF, and TGF-β1, participate in the process of pulmonary vascular remodeling in patients with pulmonary hypertension and in animal models (2, 5–8). For example, expression of EGF or its receptor EGFR are increased in animal models of monocrotaline- (MCT-) and hypoxia-induced pulmonary hypertension and in humans with pulmonary hypertension (8–10). Blockade of EGFR results in reductions in pulmonary pressure, right ventricular hypertrophy, and distal arterial muscularization in MCT-induced pulmonary hypertension (11). Moreover, PDGF and its receptor are upregulated in pulmonary arteries of patients with pulmonary hypertension (12, 13) and rodents exposed to chronic hypoxia and MCT (7, 14, 15). PDGF receptor antagonists not only prevent, but also reverse, increased right ventricular pressure and pulmonary vascular changes induced by hypoxia and MCT (13). Furthermore, the TGF-β1/Smad pathway is activated in animals with MCT- and hypoxia-induced pulmonary hypertension (6, 7) and in patients with pulmonary arterial hypertension (16). Inhibition of TGF-β1 signaling attenuates pulmonary vascular remodeling and elevated right ventricular pressure in animal models (6, 17, 18). Moreover, there is evidence of imbalanced TGF-β signaling in human pulmonary arterial hypertension (19). Despite these overwhelming data, approaches for intervention targeting these growth factors are limited, because the downstream signaling pathways originating from the activation of these growth factor receptors have not been fully characterized.

Calpain is a family of calcium-dependent, non-lysosomal neutral cysteine endopeptidases (20). There are at least 15 isozymes in the family (21, 22). Calpain-1 and calpain-2 are two major typical calpains. Calpain-1 and calpain-2 isoforms consist of a distinct larger catalytic subunit (about 80 kDa) and a common smaller subunit (about 30 kDa: calpain-4) that helps maintain calpain activity (23, 24). Calpastatin functions as the major specific endogenous inhibitor for calpain-1 and calpain-2 (20, 25, 26). Activation of calpain involves calcium, phospholipid binding, release of calpain from its inhibitor calpastatin, binding of activator proteins, and phosphorylation (27). Binding of phospholipids may decrease the Ca^{2+} requirement for calpain-2 activation (28). Calpain plays an important role in cell proliferation, migration, and differentiation of endothelial cells, fibroblasts, myoblasts, and cancerous cells through an unknown

Conflict of interest: The authors have declared that no conflict of interest exists.
Citation for this article: *J Clin Invest.* 2011;121(11):4548–4566. doi:10.1172/JCI57734.

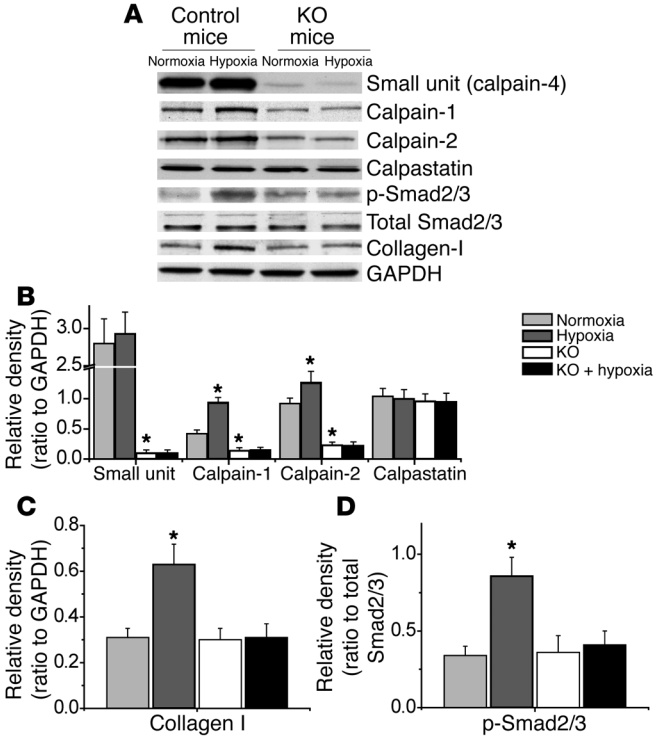

Figure 1
Protein content of calpain-1, calpain-2, calpain-4, calpastatin, p-Smad2/3, total Smad2/3, and collagen I in the lungs of *ER-Cre*$^{+/-}$*Capn4*$^{fl/fl}$ and control mice exposed to normoxia and chronic hypoxia. Five days after the regimen of tamoxifen administration, control and *ER-Cre*$^{+/-}$*Capn4*$^{fl/fl}$ mice were exposed to room air (normoxia) or 10% oxygen (hypoxia) for 3 weeks. Then protein content of calpain-1, calpain-2, calpain-4, calpastatin, p-Smad2/3, total Smad2/3, and collagen I in lung homogenates was analyzed using Western blot analysis. (**A**) Representative immunoblots from 8 experiments. (**B**–**D**) Changes in calpain-1, calpain-2, calpain-4, calpastatin, spectrin, p-Smad2/3, total Smad2/3, and collagen I quantified by scanning densitometry. Results are expressed as mean ± SEM; $n = 8$ experiments. *$P < 0.05$ versus control.

mechanism (29–32). EGF and PDGF can activate calpain-1 and calpain-2 via increased intracellular Ca^{2+} and MAP kinase activation (33–35). Recently, Gressner et al. reported that calpain can cause activation of TGF-β through an unknown mechanism (36). Because proliferation of vascular smooth muscle cells and overproduction of extracellular matrix, including collagen, are important pathological processes in pulmonary vascular remodeling (37–41), we hypothesize that calpain plays a role in collagen synthesis and cell proliferation of pulmonary artery smooth muscle cells (PASMCs) induced by growth factors in pulmonary hypertension.

In the present study, we demonstrate that calpain mediates collagen synthesis induced by EGF and PDGF via activation of intracellular TGF-β1. We found for the first time to our knowledge that conditional knockout of calpain prevents pulmonary vascular remodeling in hypoxia-induced pulmonary hypertension. More importantly, our data show that the calpain inhibitor MDL28170 prevents the progression of established pulmonary hypertension induced by MCT. These observations indicate that calpain in pulmonary vascular smooth muscle might be a novel target for intervention in pulmonary hypertension.

Results

Protein levels of calpain-1, calpain-2, calpain-4, calpastatin, SBDP, p-Smad2/3, total Smad2/3, and collagen I in the lungs of ER-Cre$^{+/-}$*Capn4*$^{fl/fl}$ *mutant and control mice exposed to normoxia and chronic hypoxia.* Our goal in the present study was to determine the role of calpain in pulmonary vascular remodeling during pulmonary hypertension. To do this, we took advantage of the *ER-Cre*$^{+/-}$*Capn4*$^{fl/fl}$ mutant mouse model. This model allows us to conditionally knock out the calpain-4 gene with administration of tamoxifen. Because calpain-4 is required for activity of calpain-1 and calpain-2, this model allows us to examine the effects of loss of calpain activity during normal and hypoxic conditions. Control and *ER-Cre*$^{+/-}$*Capn4*$^{fl/fl}$ mutant mice were treated with tamoxifen for 5 days, as described in Methods, and were then exposed to room air (normoxia) or 10% oxygen (hypoxia) for 3 weeks. As shown in Figure 1, A–D, the protein levels of calpain-1, calpain-2, p-Smad2/3, and collagen I in lungs of control mice increased during hypoxia. Moreover, the level of spectrin breakdown product (SBDP), a specific calpain degradation product, in the smooth muscle layer of pulmonary arterioles was also increased during hypoxia in control mice (Figure 2A), suggesting that hypoxia induced calpain activation in muscular pulmonary arteries. The protein levels of calpain-1, calpain-2, and calpain-4 were much lower in the lungs of *ER-Cre*$^{+/-}$*Capn4*$^{fl/fl}$ than in control mice (Figure 1). Additionally, calpain-4 protein levels were much lower in the smooth muscle layer of pulmonary arterioles of *ER-Cre*$^{+/-}$*Capn4*$^{fl/fl}$ than in control mice (Supplemental Figure 1; supplemental material available online with this article; doi:10.1172/JCI57734DS1) as were levels of the floxed *CAPN4*^{PZ} allele in the lungs (Supplemental Figure 2), indicating that deletion of the calpain-4 gene was successfully induced by tamoxifen. Knockout of calpain-4 did not affect the protein levels of calpastatin, p-Smad2/3, total Smad2/3, and collagen I under normoxic conditions (Figure 1). However, knockout of calpain-4 decreased SBDP in the smooth muscle layer of pulmonary arterioles and prevented hypoxia-induced increases in SBDP in the smooth muscle layer of pulmonary arterioles of *ER-Cre*$^{+/-}$*Capn4*$^{fl/fl}$ mice (Figure 2A), showing that calpain-4–knockout mice had impaired hypoxia-induced calpain activation. More importantly, inhibition of calpain activation prevented hypoxia-induced increases in the protein levels of calpain-1, calpain-2, collagen I, and p-Smad2/3 in *ER-Cre*$^{+/-}$*Capn4*$^{fl/fl}$ mutant mice (Figure 1). These data indicated that inhibition of calpain using conditional knockout of calpain-4 prevents collagen I accumulation and Smad2/3 phosphorylation in hypoxic mouse lungs.

Conditional knockout of calpain-4 attenuates chronic hypoxia-induced pulmonary hypertension and pulmonary vascular remodeling. As shown in Figure 3, A and B, right ventricular systolic pressure (RVSP) and the ratio of the weights of the free wall of the right ventricle to the weight of wall of left ventricle plus septum (RV/LV+S) were much higher in control mice exposed to hypoxia than those exposed to normoxia. However, RVSP and the RV/LV+S ratio were comparable in *ER-Cre*$^{+/-}$*Capn4*$^{fl/fl}$ mice exposed to normoxia and those exposed to hypoxia (Figure 3, A and B). To evaluate pulmonary vascular remodeling, we determined medial thickness of the pulmonary arterial walls and level of collagen I protein. As shown in Figure 2B and Figure 3, C and D, hypoxia for 3 weeks caused significant increases in thickness of the pulmonary vascular walls and in collagen I protein in the smooth muscle layer of pulmonary arterioles of

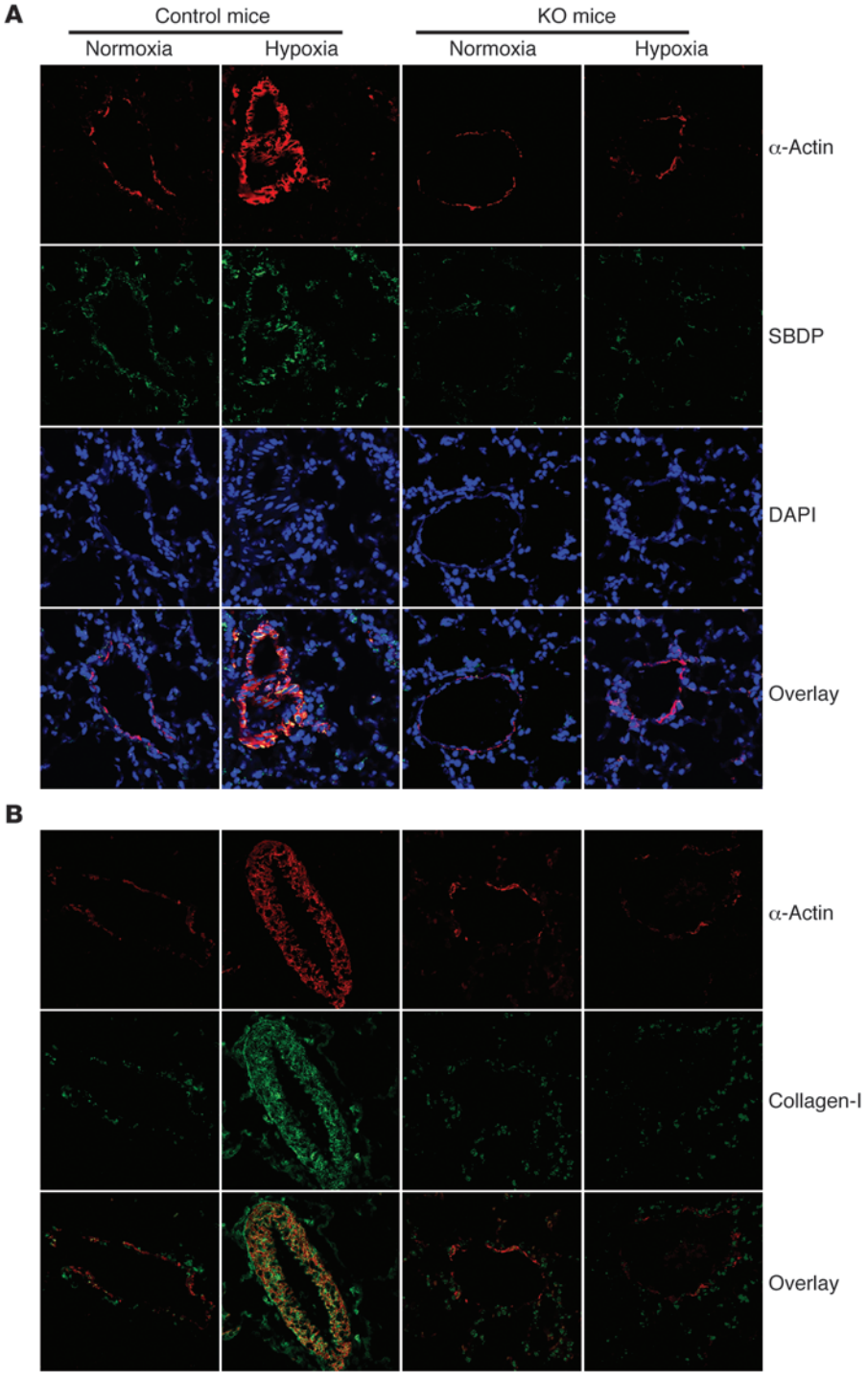

Figure 2
Effects of calpain inhibition by conditional knockout of calpain-4 on SBDP and collagen I in the smooth muscle of pulmonary arterioles of mice with hypoxic pulmonary hypertension. Five days after tamoxifen administration, control and *ER-Cre*$^{+/-}$*Capn4*$^{fl/fl}$ mice were exposed to room air (normoxia) or 10% oxygen (hypoxia) for 3 weeks. (**A**) Lung slides from *ER-Cre*$^{+/-}$*Capn4*$^{fl/fl}$ and control mice exposed to normoxia or hypoxia were double stained for α-actin (red) and SBDP (green) and then counterstained for DAPI. (**B**) Lung slides from *ER-Cre*$^{+/-}$*Capn4*$^{fl/fl}$ and control mice exposed to normoxia or hypoxia were double stained for α-actin (red) and collagen I (green). Images are representative of 8 independent experiments. Original magnification, ×400.

control mice. Hypoxia failed to increase medial thickness of the pulmonary vascular walls and expression of collagen I in the smooth muscle layer of pulmonary arterioles in calpain-4–knockout mice (Figure 2B and Figure 3, C and D). Taken together, these results indicate that inhibition of calpain by conditional knockout of calpain-4 attenuates hypoxia-induced pulmonary hypertension and pulmonary vascular remodeling.

Alterations in the amounts of EGF, PDGF-BB, active TGF-β1, and total TGF-β1 in mouse lungs of chronic hypoxia-induced pulmonary hypertension. As shown in Supplemental Figure 3, A and E, chronic hypoxia did not affect the lung levels of EGF and total TGF-β1 in control and *ER-Cre*$^{+/-}$*Capn4*$^{fl/fl}$ mice. However, levels of PDGF-BB and active TGF-β1 were increased in the lungs of control mice exposed to chronic hypoxia (Supplemental Figure 3, B–D). Conditional knockout of calpain-4 did not affect the hypoxia-induced increase in PDGF-BB content but did prevent hypoxia-induced increases in active TGF-β1 levels in lungs of *ER-Cre*$^{+/-}$*Capn4*$^{fl/fl}$ mice (Supplemental Figure 3, B–D), suggesting that knockout of calpain-4 prevents activation of TGF-β1 in hypoxic lungs.

The specific calpain inhibitor MDL28170 prevents progression of MCT-induced pulmonary hypertension and pulmonary vascular remodeling in rats. To determine whether inhibition of calpain prevents progression of established pulmonary hypertension, we examined the therapeutic effect of the specific calpain inhibitor MDL28170 on pulmonary vascular remodeling of MCT-induced pulmonary hypertension in rats. As shown in Figure 4 and Supplemental Figure 4, RVSP, RV/LV+S ratio, thickness of pulmonary vascular walls, and levels of collagen I and SBDP protein in the smooth muscle layer of pulmonary arterioles were much higher in MCT-treated rats than control rats 2 weeks after injection of MCT, indicating that pulmonary vascular remodeling and pulmonary hypertension were established. The MCT-treated rats were given MDL28170 or vehicle at the beginning of the third week after MCT treatment (Figure 4E). We found that administration of MDL28170 to control rats did not affect RVSP, RV/LV+S ratio, thickness of pulmonary vascular walls, or level of collagen I protein in the smooth

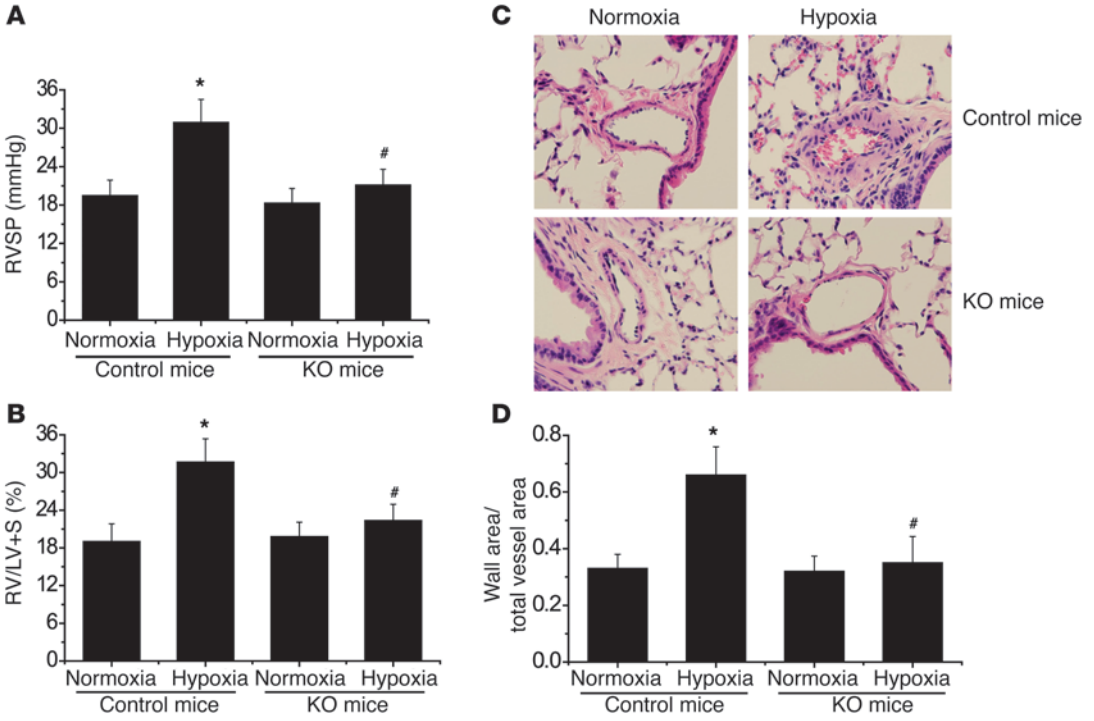

Figure 3

Conditional knockout of calpain-4 attenuates chronic hypoxia–induced pulmonary hypertension and pulmonary vascular remodeling. Five days after tamoxifen administration, control and *ER-Cre*$^{+/-}$*Capn4*$^{fl/fl}$ mice were exposed to room air (normoxia) or 10% oxygen (hypoxia) for 3 weeks. Then pulmonary hypertension and pulmonary vascular remodeling were assessed. (**A**) Changes in RVSP. (**B**) Changes in RV/LV+S. (**C**) Representative images of lung sections of control and *ER-Cre*$^{+/-}$*Capn4*$^{fl/fl}$ mice exposed to normoxia or hypoxia. Original magnification, ×400. (**D**) Changes in ratio of wall area to total vessel area in the lung sections of control and *ER-Cre*$^{+/-}$*Capn4*$^{fl/fl}$ mice exposed to normoxia or hypoxia. Results are expressed as mean ± SEM; $n = 8$ experiments. $^{*}P < 0.05$ versus normoxia; $^{\#}P < 0.05$ versus hypoxia group of control mice.

muscle layer of pulmonary arterioles (Figure 4 and Supplemental Figure 4). On the other hand, RVSP, RV/LV+S ratio, thickness of pulmonary vascular walls, and levels of collagen I and SBDP protein in the smooth muscle layer of pulmonary arterioles were much lower in MCT-treated rats injected with MDL28170 than those with vehicle injection (Figure 4 and Supplemental Figure 4). These results indicated that MDL28170 inhibits calpain activation in pulmonary arterioles of MCT-treated rats and prevents the progression of pulmonary vascular remodeling of established pulmonary hypertension induced by MCT.

Protein levels of calpain-1, calpain-2, calpain-4, calpastatin, p-Smad2/3, total Smad2/3, and collagen I in the lungs of MCT-treated, MDL28170-treated, and control rats. As shown in Supplemental Figure 5, the protein levels of calpain-1 were slightly higher and the protein levels of collagen I and p-Smad2/3 were much higher in the lungs of MCT-treated rats compared with controls. Moreover, the specific calpain degradation product SBDP was increased in the smooth muscle layer of pulmonary arterioles in MCT-treated rats (Supplemental Figure 4B), suggesting that calpain is activated in pulmonary arterioles of MCT-treated rats. Inhibition of calpain using MDL28170 slightly decreased the protein levels of calpain-1 and calpain-2 and did not affect the levels of calpain-4, calpastatin, p-Smad2/3, total Smad2/3, and collagen I in control rats (Supplemental Figure 5). However, MDL28170 inhibited the increase in SBDP in the smooth muscle layer of pulmonary arterioles of MCT-treated rats (Supplemental Figure 4B). More importantly, inhibition of calpain activation using MDL28170 ameliorated progressive increases in the protein levels of collagen I and p-Smad2/3 in the lungs of MCT-treated rats (Supplemental Figure 5, A, C, and D). These data indicated that inhibition of calpain using MDL28170 prevents collagen I accumulation and Smad2/3 phosphorylation in lungs of rats with MCT-induced pulmonary hypertension.

Alterations in the levels of EGF, PDGF-BB, active TGF-β1, and total TGF-β1 in the lungs of MCT- and MDL28170-treated rats. As shown in Supplemental Figure 6, the levels of EGF, PDGF-BB, active TGF-β1, and total TGF-β1 were higher in lungs of MCT-treated rats than control rats 3 weeks after injection. The magnitude of increase in active TGF-β1 was higher than that for total TGF-β1, suggesting that activation of TGF-β1 was enhanced in lungs of MCT-treated rats. Administration of MDL28170 during the third week did not affect increases in EGF, PDGF-BB, and total TGF-β1 but inhibited the increase in active TGF-β1 (Supplemental Figure 6), indicating that inhibition of calpain prevents activation of TGF-β1 in lungs of MCT-treated rats.

EGF and PDGF-BB increase calpain activity, collagen synthesis, and cell proliferation in PASMCs. To determine the mechanism for calpain-mediated pulmonary vascular remodeling, we examined the effects of EGF and PDGF-BB on calpain activity, collagen synthesis, and cell proliferation in PASMCs. We found that incubation of cells with EGF and PDGF-BB for 1 hour induced dose-dependent increases in calpain activity (Figure 5, A and E). Moreover, incubation of PASMCs with EGF and PDGF-BB for 24 hours caused dose-dependent increases in intracellular collagen I protein level, *COL1A1* mRNA level, and cell proliferation (Figure 5, B–D and F–H). The

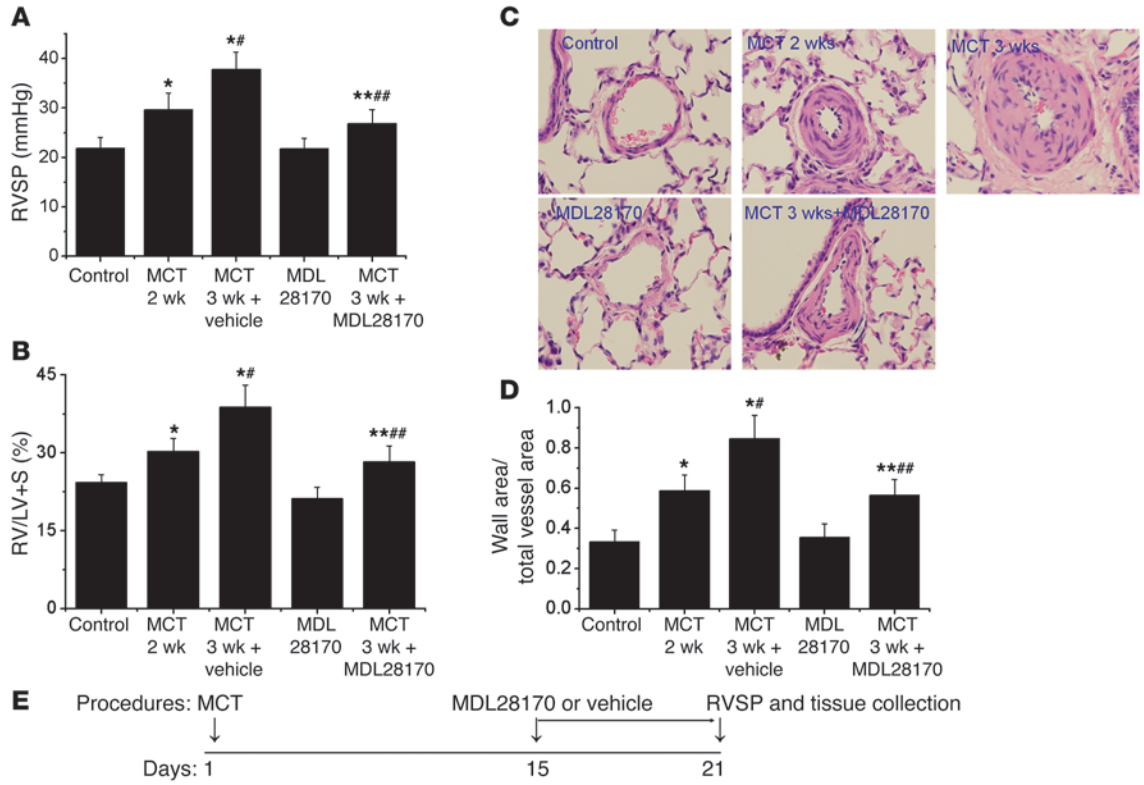

Figure 4

The specific calpain inhibitor MDL28170 prevents progression of MCT-induced pulmonary hypertension and pulmonary vascular remodeling in rats. Male Sprague-Dawley rats 8 weeks of age were injected subcutaneously without or with MCT (60 mg/kg). After 2 weeks, pulmonary hypertension and pulmonary vascular remodeling were determined in control and MCT-injected rats (MCT 2 weeks). At the same time (the beginning of third week), groups of control rats (MDL28170) and MCT-injected rats (MCT 3 wk + MDL28170) began receiving MDL28170 (20 mg/kg, i.p.) once daily. A second group of MCT-injected rats received the same volume of vehicle (MCT 3 wk). Pulmonary hypertension and pulmonary vascular remodeling were assessed 1 week later (3 weeks after MCT injection). (**A**) Changes in RVSP. (**B**) Changes in RV/LV+S. (**C**) Representative images of lung sections of rats. Original magnification, ×400. (**D**) Changes in ratio of wall area to total vessel area in the lung sections of rats. (**E**) Protocol for time course of this experiment. Results are expressed as mean ± SEM; $n = 6$ experiments. $^{*}P < 0.05$ versus control; $^{**}P < 0.05$ versus MDL28170; $^{\#}P < 0.05$ versus MCT 2 wk; $^{\#\#}P < 0.05$ versus MCT 3 wk.

alterations in level of intracellular collagen I protein are in line with the levels of collagen I protein in culture medium, suggesting that collagen I is secreted into extracellular space. The increases in the protein and mRNA levels of collagen I were not due to increases in the number of cells caused by increased proliferation, as these results were normalized to internal control levels of GAPDH or 18S RNA.

Inhibition of calpain using the specific calpain inhibitor MDL28170 and siRNAs against calpain-1 and calpain-2 block EGF- and PDGF-BB–induced increases in collagen synthesis and proliferation of PASMCs. To investigate the role of calpain on EGF- and PDGF-BB–induced increases in collagen synthesis and cell proliferation, we incubated PASMCs with or without EGF and PDGF-BB (10 ng/ml) in the presence and absence of MDL28170 (20 μM) for 24 hours, after which protein levels of intracellular collagen I, *COL1A1* mRNA levels, and cell proliferation were measured. As shown in Figure 6, increases in levels of collagen protein, *COL1A1* mRNA, and cell proliferation induced by EGF and PDGF-BB were blocked by the presence of MDL28170, indicating that calpain is involved in the EGF- and PDGF-BB–induced increases in collagen synthesis and proliferation of PASMCs.

To investigate which isoform of calpain (calpain-1 or calpain-2) is involved in EGF- and PDGF-BB–induced increases in collagen synthesis and cell proliferation, we knocked down expression of calpain-1 or calpain-2 proteins in PASMCs using their siRNAs. As shown in Figure 7A, transfection of PASMCs with siRNA targeting the mRNA of calpain-1 or calpain-2 significantly reduced the protein levels of calpain-1 or calpain-2 without affecting the expression of calpain small unit (calpain-4) or calpastatin. Knocking down the protein expression of calpain-1 or calpain-2 prevented EGF-induced increases in calpain activity (Figure 7B), intracellular collagen I protein levels (Figure 7, C and D), and cell proliferation (Figure 7E). These results suggest that calpain-1 and calpain-2 act cooperatively and play important roles in mediating EGF- and PDGF-BB–induced increases in collagen synthesis and cell proliferation of PASMCs.

EGF and PDGF increase intracellular active TGF-β1 and phosphorylation of Smad2/3 in PASMCs. To study the effects of EGF and PDGF on the activation of TGF-β1, we incubated PASMCs with PDGF-BB (10 ng/ml) for 0.5–24 hours and then measured intracellular levels of active TGF-β1, p-Smad2/3, total Smad2/3, and intracellular collagen I by Western blot analysis. As shown in Figure 8, A and B, incubation of PASMCs with PDGF-BB increased intracellular active TGF-β1 at 0.5–12 hours, p-Smad2/3 at 2–4 hours, and collagen I at 12–24 hours. The time course of the increase in intracellular active TGF-β1 corresponded with that of calpain activity (Figure 8C), suggesting that calpain is

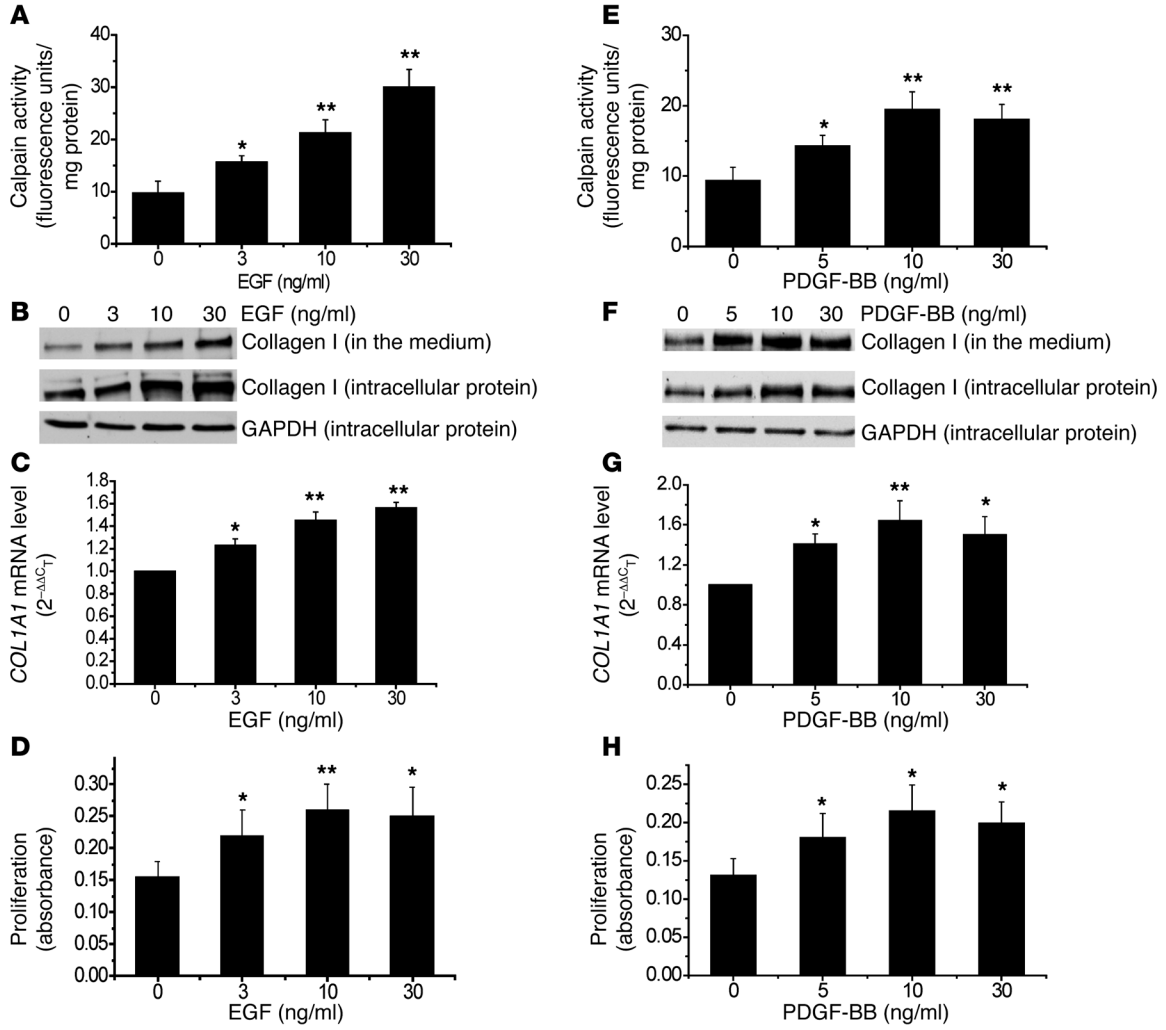

Figure 5

EGF and PDGF increase calpain activity, collagen synthesis, and cell proliferation in PASMCs. PASMCs were incubated with EGF and PDGF-BB (3–30 ng/ml) for 1–24 hours, after which calpain activity (**A** and **E**), collagen I protein content in the cell lysates and culture medium (**B** and **F**), *COL1A1* mRNA (**C** and **G**), and cell proliferation (**D** and **H**) were measured as described in Methods. (**B** and **F**) Representative immunoblots from 4 experiments. Results are expressed as mean ± SEM; $n = 4$ experiments. $^*P < 0.05$, $^{**}P < 0.01$ versus control (0 ng/ml).

involved in the activation of intracellular TGF-β1. To further confirm EGF- and PDGF-BB–induced activation of TGF-β1, we determined levels of active TGF-β1 and total TGF-β1 in the cells and in the medium using a TGF-β1 ELISA. We found that incubation of PASMCs with EGF and PDGF-BB (10 ng/ml) for 2 hours increased intracellular active TGF-β1 (Figure 8, D and E). However, levels of intracellular total TGF-β1 as well as active TGF-β1 and total TGF-β1 in the medium were comparable between EGF- and PDGF-BB–treated cells and control cells (Figure 8, D and E). These data suggest that EGF- and PDGF-BB–induced collagen synthesis occurs through activation of intracellular TGF-β1.

Effects of anti–TGF-β neutralizing antibody, SB431542, and the Smad2/3 inhibitor SIS3 on EGF- and PDGF-BB–induced phosphorylation of Smad2/3 and collagen synthesis in PASMCs. To further confirm the role of activation of intracellular TGF-β1 in EGF- and PDGF-BB–induced collagen synthesis, we cultured PASMCs in Transwell inserts with 0.4-μm pores. A cell-impermeable anti–TGF-β neutralizing antibody was added to the culture medium in and underneath the inserts to neutralize TGF-β1 in the extracellular space. As shown in Figure 9, A and B, and Figure 10, A and B, this anti–TGF-β neutralizing antibody did not affect EGF- and PDGF-BB–induced phosphorylation of Smad2/3 and collagen synthesis in PASMCs. However, the anti–TGF-β neutralizing antibody blocked the effect of active TGF-β1 when it was added in the culture medium (Supplemental Figure 7). In contrast, the cell-permeable TGF-β1 receptor Alk5 inhibitor SB431542 prevented EGF- and PDGF-BB–induced phosphorylation of Smad2/3 and collagen synthesis (Figure 9, C and D, and Figure 10, C and D). These results provide additional evidence that EGF and PDGF-BB induce intracellular activation of TGF-β1. Furthermore, the Smad3 inhibitor SIS3 prevented EGF- and PDGF-BB–induced phosphorylation of Smad2/3 and collagen synthesis (Figure 9, E and F, and Figure 10, E and F), suggesting that intracellular activation of TGF-β1 causes collagen synthesis through Smad2/3 signaling.

Inhibition of calpain blocks EGF- and PDGF-BB–induced increases in intracellular active TGF-β1 and phosphorylation of Smad2/3 in PASMCs. As shown in Figure 11A, incubation of PASMCs with MDL28170 pre-

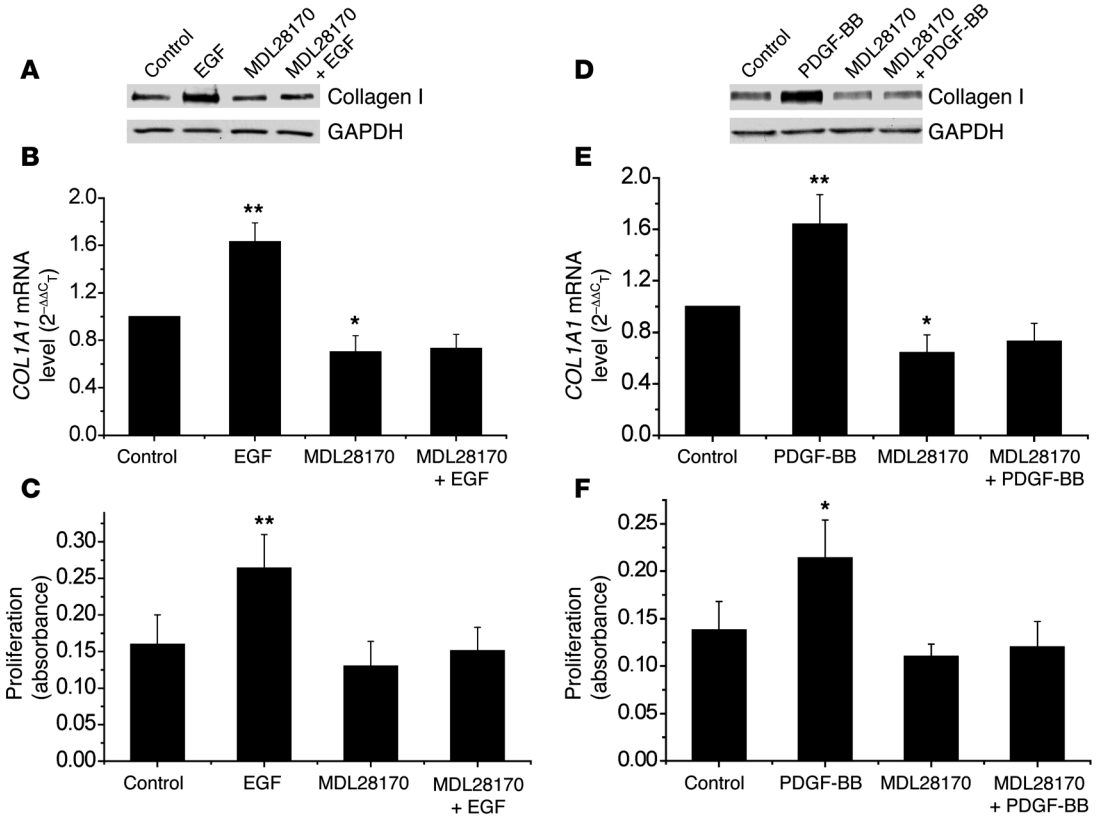

Figure 6
Specific calpain inhibitor MDL28170 inhibits EGF- and PDGF-BB–induced increases in collagen synthesis and cell proliferation of PASMCs. PASMCs were incubated with EGF (10 ng/ml) and PDGF-BB (10 ng/ml) in the presence and absence of MDL28170 (20 μM) for 24 hours, after which intracellular collagen I protein content (**A** and **D**), *COL1A1* mRNA (**B** and **E**), and cell proliferation (**C** and **F**) were measured as described in Methods. (**A** and **D**) Representative immunoblots from 4 experiments. Results are expressed as mean ± SEM; $n = 4$ experiments. $^*P < 0.05$, $^{**}P < 0.01$ versus control.

vented EGF-induced increase in intracellular active TGF-β1, as determined by Western blot analysis. Similar data were obtained when intracellular active TGF-β1 was assayed using ELISA (Figure 11B). Moreover, the increases in intracellular active TGF-β1 induced by PDGF-BB was also prevented by MDL28170 (Figure 11C). Furthermore, inhibition of calpain using MDL28170 or siRNAs against calpain-1 and calpain-2 prevented EGF- or PDGF-BB–induced phosphorylation of Smad2/3 (Figures 11, D–I). Together, these results indicate that intracellular activation of TGF-β1 caused by calpain initiates Smad2/3 signaling in EGF- and PDGF-BB–treated PASMCs.

Colocalization of active TGF-β, Alk5, and calpain in the Golgi of PDGF-BB–treated PASMCs. To determine whether the intracellular localization of active TGF-β, Alk5, and calpain is in the Golgi, we incubated PASMCs with PDGF-BB for 30 minutes. The cells were then double stained for Golgi and active TGF-β, Alk5 and active TGF-β, or Golgi and calpain-1. We found that active TGF-β was colocalized in the Golgi of cells treated with PDGF-BB for 30 minutes (Figure 12A). MDL28170 prevented the PDGF-BB–induced increase in active TGF-β in the Golgi (Figure 12A). Furthermore, incubation of PASMCs with PDGF-BB for 30 minutes caused an increase in colocalization of calpain-1 in the Golgi (Figure 12B). Importantly, we found that active TGF-β was colocalized with Alk5 in PDGF-BB–treated PASMCs (Figure 12C). The increase in Alk5 in the Golgi was not due to an increase in the protein level of Alk5, because this was comparable in PDGF-BB–treated and control cells (Supplemental Figure 11B). Together, these results indicate that a calpain-activated intracellular TGF-β signaling pathway truly exists in PASMCs.

Calpain-1 and -2 activate latent TGF-β1 in vitro. To determine whether calpain activates TGF-β1 by cleavage of latent TGF-β1, we incubated purified latent TGF-β1 overnight with calpain-1 (0–158 U/ml) or calpain-2 (0–173 U/ml) in the presence of 5 mM calcium. Active TGF-β1 in the mixture was assayed using Western blot and ELISA. As shown in Figure 13, incubation of latent TGF-β1 with calpain-1 and -2 caused concentration-dependent increases in the cleavage of latent TGF-β1 and in active TGF-β1. The effects of calpain-1 and -2 could be prevented by MDL28170. These results indicate that calpain activates TGF-β1 by cleaving latent TGF-β1.

EGF, PDGF, and MDL28170 do not affect apoptosis and protein levels of PTEN, PP2A-B56-α, and PP2A-56-β in PASMCs. To rule out the possibility that calpain-mediated collagen synthesis and intracellular TGF-β1 activation are due to changes in apoptosis and levels of phosphatase and tensin homolog on chromosome 10 (PTEN), protein phosphatase 2A-B56-α (PP2A-B56-α), and PP2A-56-β, we examined apoptosis and protein levels of PTEN, PP2A-B56-α, and PP2A-56-β in PASMCs incubated with PDGF-BB, EGF, or MDL28170. We found that PDGF-BB (10 ng/ml, 24 hours) and MDL28170 (20 μM, 24 hours) did not cause any changes in FITC–

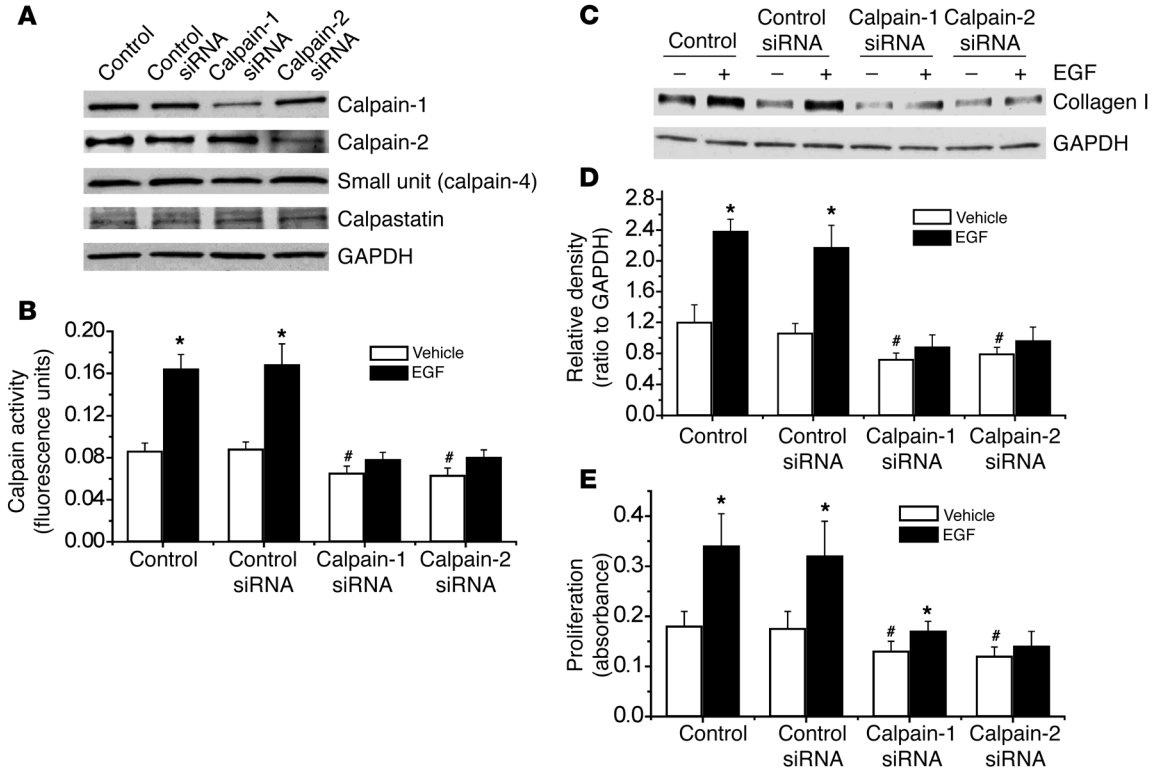

Figure 7

Knockdown of calpain-1 and calpain-2 attenuates EGF-induced increases in calpain activity, collagen synthesis, and cell proliferation. PASMCs were transfected with an siRNA against the mRNA of calpain-1, calpain-2, or control (luciferase) siRNA. After 96 hours, the cells were incubated with EGF (10 ng/ml) for 1–24 hours, and then protein content of calpain-1, calpain-2, small unit (calpain-4), and calpastatin (**A**); calpain activity (**B**); intracellular collagen I protein content (**C** and **D**); and cell proliferation (**E**) were measured as described in Methods. (**A** and **C**) Representative immunoblots of calpain-1, calpain-2, calpain-4, calpastatin, and collagen I from 4 experiments. (**D**) Changes in the intracellular collagen I protein content quantified by scanning densitometry. Results are expressed as mean ± SEM; $n = 4$ experiments. $^{*}P < 0.05$ versus vehicle (without EGF); $^{\#}P < 0.05$ versus vehicle (without EGF) in control siRNA.

active caspase-3 in PASMCs (Supplemental Figure 8). Moreover, incubation of PASMCs with EGF (10 ng/ml) or MDL28170 (20 μM) for 24 hours did not affect protein levels of PTEN, PP2A-B56-α, or PP2A-56-β in PASMCs (Supplemental Figure 9). These data indicate that calpain-mediated collagen synthesis and intracellular TGF-β1 activation are not due to changes in apoptosis and levels of PTEN, PP2A-B56-α, and PP2A-56-β.

Effects of neutralizing anti–TGF-β antibody and the Alk5 inhibitor SB431542 on chronic hypoxia-induced pulmonary hypertension and pulmonary vascular remodeling. We further investigated whether intracellular TGF-β1 activation and signaling occur in pulmonary vascular remodeling and pulmonary hypertension in vivo. Mice were exposed to room air (normoxia) or 10% oxygen (hypoxia). At the beginning of the second week, groups of normoxic and hypoxic mice were injected with neutralizing anti–TGF-β antibody or SB431542. Three weeks after hypoxia, plasma TGF-β1 levels, pulmonary hypertension, and pulmonary vascular remodeling were assessed. As shown in Figure 14, cell-impermeable neutralizing anti–TGF-β antibody dramatically decreased the level of active TGF-β1 in plasma, but it failed to block chronic hypoxia–induced increases in RVSP, RV/LV+S ratio, and thickness of pulmonary arterial walls. However, the cell-permeable TGF-β1 receptor Alk5 inhibitor SB431542 prevented chronic hypoxia–induced increases in RVSP, RV/LV+S ratio, and thickness of pulmonary arterial walls (Figure 14). The aggregate results, which agree with our prior observations in the MCT model of pulmonary hypertension (17), suggest that it is intracellular TGF-β1, which is activated by calpain, that mediates pulmonary vascular remodeling and pulmonary hypertension induced by hypoxia.

Higher levels of calpain activation and active TGF-β in smooth muscle cells of muscular pulmonary arteries of patients with pulmonary arterial hypertension. To address the clinical relevance of these observations in animal models, we determined levels of the specific calpain cleavage product SBDP and of active TGF-β in smooth muscle cells of pulmonary arteries. As shown in Figure 15, the smooth muscle cells of pulmonary arteries of patients with idiopathic pulmonary arterial hypertension contained higher levels of SBDP, a specific calpain degradation product, and active TGF-β, findings that are also in line with our prior data (19). Together, these results indicate that calpain activity and active TGF-β are increased in smooth muscle cells of pulmonary arterioles in patients with pulmonary hypertension.

Knockout of calpain-4 decreases endothelium-dependent relaxation and smooth muscle contractility. As shown in Supplemental Figure 10, A and B, endothelium-dependent relaxation induced by acetylcholine was much lower in pulmonary arteries from *ER-Cre*$^{+/-}$*Capn4*$^{fl/fl}$ mice than control mice. However, smooth muscle contraction induced by phenylephrine was reduced in pulmonary arteries from

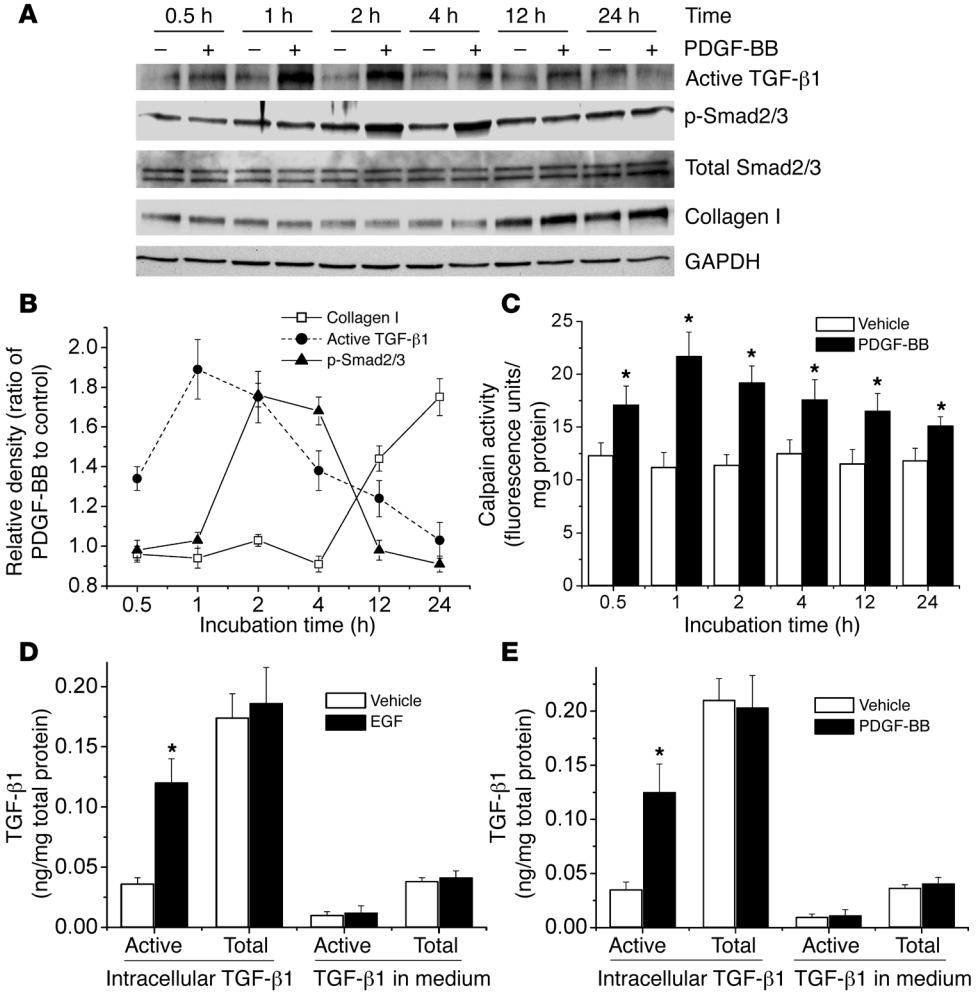

Figure 8

EGF and PDGF-BB induce increases in intracellular active TGF-β1 and phosphorylation of Smad2/3 in PASMCs. (**A**) Representative immunoblots of intracellular active TGF-β1, p-Smad2/3, total Smad2/3, and collagen I in the lysates of PASMCs incubated with or without PDGF-BB (10 ng/ml) for 0.5–24 hours. (**B**) Changes in intracellular active TGF-β1, p-Smad2/3, and collagen I protein content quantified by scanning densitometry. (**C**) Time-dependent changes in calpain activity in PASMCs incubated with or without PDGF-BB (10 ng/ml) for 0.5–24 hours. (**D**) ELISA assay of the content of active TGF-β1 and total TGF-β1 in the lysates and medium of PASMCs incubated with or without EGF (10 ng/ml) for 2 hours. (**E**) ELISA assay of the content of active TGF-β1 and total TGF-β1 in the lysates and medium of PASMCs incubated with or without PDGF-BB (10 ng/ml) for 2 hours. Results are expressed as mean ± SEM; $n = 4$ experiments. *$P < 0.05$ versus vehicle (without EGF or PDGF).

ER-Cre$^{+/-}$*Capn4*$^{fl/fl}$ mice (Supplemental Figure 10, C and D). Knockout of calpain-4 did not affect NO donor sodium nitroprusside–induced (SNP-induced) relaxation (Supplemental Figure 10E).

Effects of PDGF-BB and MDL28170 on cell migration and protein levels of CTGF and Alk5 in PASMCs. As shown in Supplemental Figure 11, A and B, PDGF-BB induced increases in cell migration and connective tissue growth factor (CTGF) protein levels in PASMCs. These increases could be inhibited by MDL28170. PDGF-BB and MDL28170 did not affect Alk5 protein levels in PASMCs (Supplemental Figure 11B).

Discussion

We show here that calpain plays an important role in hypoxia- and MCT-induced pulmonary vascular remodeling and pulmonary hypertension. We found for the first time to our knowledge that inhibition of calpain activity by conditional knockout of calpain-4 prevented hypoxia-induced pulmonary vascular remodeling and pulmonary hypertension. In addition, the specific calpain inhibitor MDL28170 prevented the progression of established pulmonary hypertension induced by MCT. In PASMCs, inhibition of calpain using MDL28170 or calpain-1 and -2 siRNAs attenuated EGF- and PDGF-induced collagen synthesis and cell proliferation. Furthermore, both EGF and PDGF induced increases in intracellular active TGF-β1 and p-Smad2/3, but not active or total extracellular TGF-β1 in the culture medium. EGF- or PDGF-induced collagen synthesis was not prevented by cell-impermeable TGF-β neutralizing antibody but was by the cell-permeable Alk5 inhibitor SB431542 and Smad2/3 inhibitor SIS3. Additionally, calpain inhibition blocked EGF- and PDGF-induced increases in active intracellular TGF-β1 and p-Smad2/3. More interestingly, active TGF-β induced by PDGF-BB colocalized with Alk5 in the Golgi. Thus, these observations indicate that calpain mediates collagen synthesis induced by EGF and PDGF via activation of intracellular TGF-β1 (Supplemental Figure 12).

To examine the role of calpain in the pathogenesis of pulmonary hypertension, we used two animal models: a hypoxic mouse model and an MCT-induced rat model. We found that conditional knockout of calpain-4 caused decreases in the levels of calpain-4 protein and the specific calpain degradation product SBDP in pulmonary artery smooth muscle layers, indicating that calpain inhibition was achieved. Because calpain activity is required for calpain gene expression (42), the calpain-4 knockout also decreased calpain-1 and -2 protein levels. Thus, besides reduction of calpain-4, decreases in calpain-1 and -2 may also contribute to the inhibition of calpain activity in *ER-Cre*$^{+/-}$*Capn4*$^{fl/fl}$ mice. Our results indicate that calpain-4 knockout results in impairment of hypoxia-induced calpain activation and prevents over-deposition of collagen I and thickening of the smooth muscle layer of pulmonary arterioles in the lungs of hypoxic mice. More importantly, the calpain-4 knockout attenuates increases in RVSP and thickness of the right ventricular wall. These data indicate that inhibition of calpain prevents pulmonary

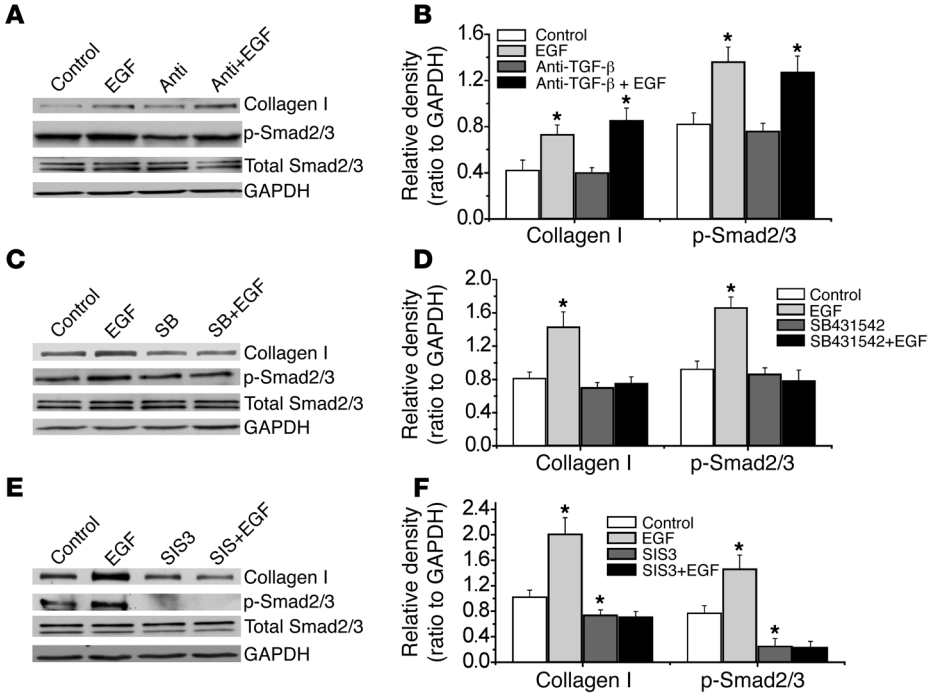

Figure 9
Effects of anti–TGF-β neutralizing antibody, the TGF-β1 receptor inhibitor SB431542, and the Smad2/3 inhibitor SIS3 on EGF-induced phosphorylation of Smad2/3 and intracellular collagen I protein content in PASMCs. PASMCs were incubated with EGF (**A**–**F**, 10 ng/ml) in the presence and absence of anti–TGF-β neutralizing antibody (1 μg/ml), SB431542 (10 μM), and SIS3 (10 μM) for 4 hours (p-Smad2/3, total Smad2/3), or 24 hours (collagen I protein), after which p-Smad2/3, total Smad2/3, and collagen I protein were measured using Western blot analysis. (**A**, **C**, and **E**) Representative immunoblots of 4 experiments. (**B**, **D**, and **F**) Changes in p-Smad2/3 and collagen I protein content quantified by scanning densitometry. Results are expressed as mean ± SEM; $n = 4$ experiments. $^*P < 0.05$ versus vehicle (without EGF). Anti, anti–TGF-β neutralizing antibody; SB, SB431542.

vascular remodeling in hypoxia-induced pulmonary hypertension. In the MCT-induced pulmonary hypertension model, we observed a progressive increase in SBDP levels in the smooth muscle layer of pulmonary arterioles, suggesting that calpain is activated in the pulmonary artery of rats receiving MCT. Administration of MDL28170 to rats with established pulmonary hypertension prevented MCT-induced calpain activation and inhibited increases in RVSP and wall thickness of the pulmonary artery and right ventricle and in collagen I protein in the smooth muscle layer of pulmonary arterioles. These results indicate that calpain inhibition prevents the progression of pulmonary vascular remodeling of established pulmonary hypertension induced by MCT.

EGF and its receptor EGFR have been reported to participate in the process of pulmonary vascular remodeling in animal models of pulmonary hypertension (2, 5–8). Sheng et al. (10) reported that hypobaric hypoxia increases EGFR protein expression in pulmonary arteries of ovine fetuses and that hypoxia-induced proliferation of fetal ovine pulmonary vascular smooth muscle cells can be prevented by the EGFR inhibitor AG1478. Merklinger et al. (11) found that the EGFR inhibitor PKI166 reverses established MCT-induced pulmonary hypertension in rats. Dahal et al. (43) reported that the EGFR inhibitors gefitinib, erlotinib, and lapatinib reduce pulmonary vascular remodeling in a model of established pulmonary hypertension induced by MCT, but not in mice with chronic hypoxia. Our data show that chronic hypoxia does not increase EGF levels in mouse lungs, but EGF levels are increased in rat lungs of MCT-induced pulmonary hypertension. Together the results indicate that EGF signaling contributes to MCT-induced pulmonary hypertension, but its role in hypoxia-induced pulmonary hypertension remains unclear.

PDGF and its receptor are upregulated in pulmonary arteries of patients with pulmonary hypertension (12, 13) and rodents exposed to chronic hypoxia and MCT (7, 14, 15). The PDGF receptor antagonist STI571 (imatinib) is reported to prevent or reverse elevated right ventricular pressure and pulmonary vascular changes induced by hypoxia and MCT (13). Consistent with this observation, we found that PDGF-BB was increased in lungs of mice exposed to chronic hypoxia and lungs of rats treated with MCT. Thus, it appears that there is agreement regarding the role of PDGF signaling in both hypoxia- and MCT-induced pulmonary hypertension.

EGF and PDGF have been reported to activate calpain-1 and calpain-2 (33, 44, 45). The mechanism is related to increased intracellular Ca^{2+} and MAP kinase activation through EGF and PDGF receptors (33–35). In this study, we have demonstrated that treatment with EGF or PDGF-BB increases calpain activity, collagen I synthesis, and cell proliferation in PASMCs. We have also shown that inhibition of calpain by calpain inhibitor or by siRNA directed against calpain-1 or calpain-2 attenuates EGF- and PDGF-BB–induced increases in calpain activity, cell proliferation, and collagen I synthesis in PASMCs. These data provide the first evidence to our knowledge that calpain-1 and calpain-2 play a mediating role in EGF- and PDGF-BB–induced collagen I synthesis and cell proliferation in PASMCs.

We further studied the signaling pathway downstream of calpain in EGF- and PDGF-induced collagen I synthesis and cell proliferation in PASMCs. Calpain can be proapoptotic or antiapoptotic depending on the inducers (46). However, we did not observe any changes in FITC–active caspase-3 in PDGF-BB– or MDL28170-treated PASMCs (Supplemental Figure 8), indicating that an alteration in apoptosis is unlikely to contribute to calpain-regulated collagen I synthesis and cell proliferation. On the other hand, calpain acts via limited proteolysis of substrate proteins. Several proteins that regulate collagen synthesis, such as PTEN and PP2A, have been reported to be the substrates for calpain (47, 48). PTEN has been reported to be a potent endogenous inhibitor of collagen synthesis (49). However, we did not observe any changes in the protein levels of PTEN or PP2A in EGF- and PDGF-BB–treated PASMCs (Supplemental Figure 9), suggesting that PTEN or PP2A are unlikely to be involved downstream of calpain in EGF- and PDGF-induced collagen I synthesis.

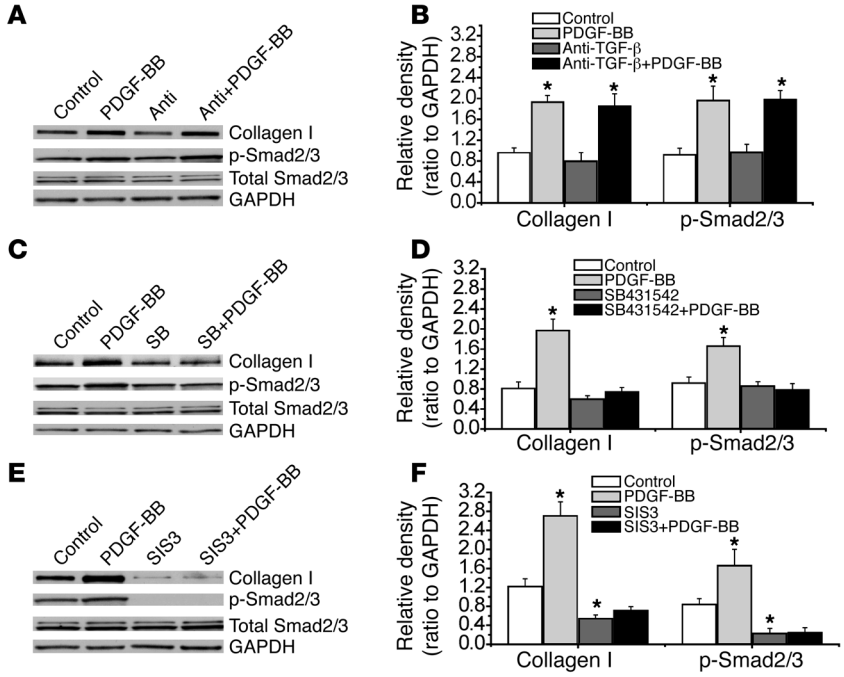

Figure 10
Effects of anti–TGF-β neutralizing antibody, the TGF-β1 receptor inhibitor SB431542, and the Smad2/3 inhibitor SIS3 on PDGF-BB–induced phosphorylation of Smad2/3 and intracellular collagen I protein content in PASMCs. PASMCs were incubated with PDGF-BB (**A**–**F**, 10 ng/ml) in the presence and absence of anti–TGF-β neutralizing antibody (1 μg/ml), SB431542 (10 μM), and SIS3 (10 μM) for 4 hours (p-Smad2/3, total Smad2/3) or 24 hours (collagen I protein), after which p-Smad2/3, total Smad2/3, and collagen I protein were measured using Western blot analysis. (**A**, **C**, and **E**) Representative immunoblots of 4 experiments. (**B**, **D**, and **F**) Changes in p-Smad2/3 and collagen I protein content quantified by scanning densitometry. Results are expressed as mean ± SEM; $n = 4$ experiments. *$P < 0.05$ versus control (without PDGF-BB).

Interestingly, Abe et al. reported that latent TGF-β1 is a substrate of calpain and that calpain activates TGF-β1 by cleaving latency-associated peptide (LAP) on the surface of endothelial cells when exogenous calpain is added to the culture medium (50). TGF-β1 is synthesized as an inactive latent precursor, termed the small latent TGF-β1 complex, that is composed of an N-terminal LAP and a C-terminal mature TGF-β1. After secretion from the cells, the small latent TGF-β1 complex binds to a latent TGF-β1 binding protein (LTBP) that directs the localization of the latent complex to the extracellular matrix. To test the possibility that calpain-mediated collagen I synthesis may involve the activation of TGF-β1 on the surface or in the medium of PASMCs, we measured calpain activity and content of active and total TGF-β1 in the medium and cell lysates of PASMCs. We found that calpain activity was too low to be detected in the culture medium. The levels of active and total TGF-β1 in the medium were not affected by EGF and PDGF-BB (Figure 8). However, the levels of active TGF-β1 in the cell lysates were increased in EGF- and PDGF-treated cells. Moreover, EGF- and PDGF-BB–induced increases in collagen I synthesis and Smad2/3 phosphorylation were prevented by cell-permeable specific inhibitors of Alk5 (SB431542) or Smad2/3 (SIS3) but not by cell-impermeable TGF-β1 neutralizing antibody. Thus, it is unlikely that TGF-β1 is activated on the surface or in the medium of PASMCs. Our data support a novel concept whereby EGF and PDGF-BB induce intracellular activation of TGF-β1, which initiates the Smad2/3 signaling pathway, leading to collagen synthesis and proliferation of PASMCs.

We further determined whether intracellular activation of TGF-β1 is mediated by calpain. We found that incubation of purified latent TGF-β1 with calpain-1 or -2 caused cleavage of latent TGF-β1 and release of active TGF-β1. The specific calpain inhibitor MDL28170 and siRNAs against calpain-1 and calpain-2 attenuated EGF- and PDGF-BB–induced increases in intracellular active TGF-β1 and Smad2/3 phosphorylation in PASMCs (Figure 11). Taken together, these observations support the hypothesis that an intracrine TGF-β1 signaling pathway exists in PASMCs. EGF- and PDGF-induced activation of calpain initiates this intracrine TGF-β1 signaling pathway, which plays an important role in EGF- and PDGF-BB–induced collagen I synthesis and proliferation in PASMCs.

The small latent TGF-β1 complex and TGF-β1 receptors are processed in the Golgi complex and endoplasmic reticulum. The small latent TGF-β1 complex and TGF-β receptors are from either de novo synthesis or clathrin-mediated endocytosis (51). The small latent TGF-β1 complex does not bind to TGF-β receptors without prior activation. Our data show that latent TGF-β1 can be activated intracellularly in PASMCs. Notably, intracellular activation of the small latent TGF-β1 complex has also been observed in plasma cells of autoimmune mice (52) and in hepatocytes of injured liver (36). Interestingly, calpain colocalizes in the Golgi complex and endoplasmic reticulum (53). Thus, it is possible that the small latent TGF-β1 complex in the Golgi complex or endoplasmic reticulum could be activated by calpain. To test this possibility, we determined the intracellular localization of active TGF-β, Alk5, and calpain in PDGF-BB–treated PASMCs. We found that active TGF-β was colocalized in the Golgi of PDGF-BB–treated cells and that MDL28170 prevented the PDGF-BB–induced increase in active TGF-β in the Golgi. Furthermore, PDGF-BB caused an increase in colocalization of calpain-1 in the Golgi and colocalization of active TGF-β and Alk5 in PASMCs. Therefore, a calpain-activated intracellular TGF-β signaling pathway truly exists in PASMCs (Supplemental Figure 12). Nevertheless, intracellular binding of TGF-β to its receptor may reduce TGF-β and its receptor trafficking to the cell surface (54) and diminish the effect of extracellular TGF-β on smooth muscle cells. Further investigations are needed to test this possibility.

In our in vivo studies, we found that inhibition of calpain by conditional knockout of calpain-4 did not significantly affect the increase in hypoxia-induced PDGF-BB but did prevent increases in active TGF-β1 and p-Smad2/3. Similarly, inhibition of calpain using MDL28170 did not affect the increase in PDGF-BB but did prevent increases in active TGF-β1 and p-Smad2/3 in lungs of rats treated with MCT. These results suggest that the calpain-mediated

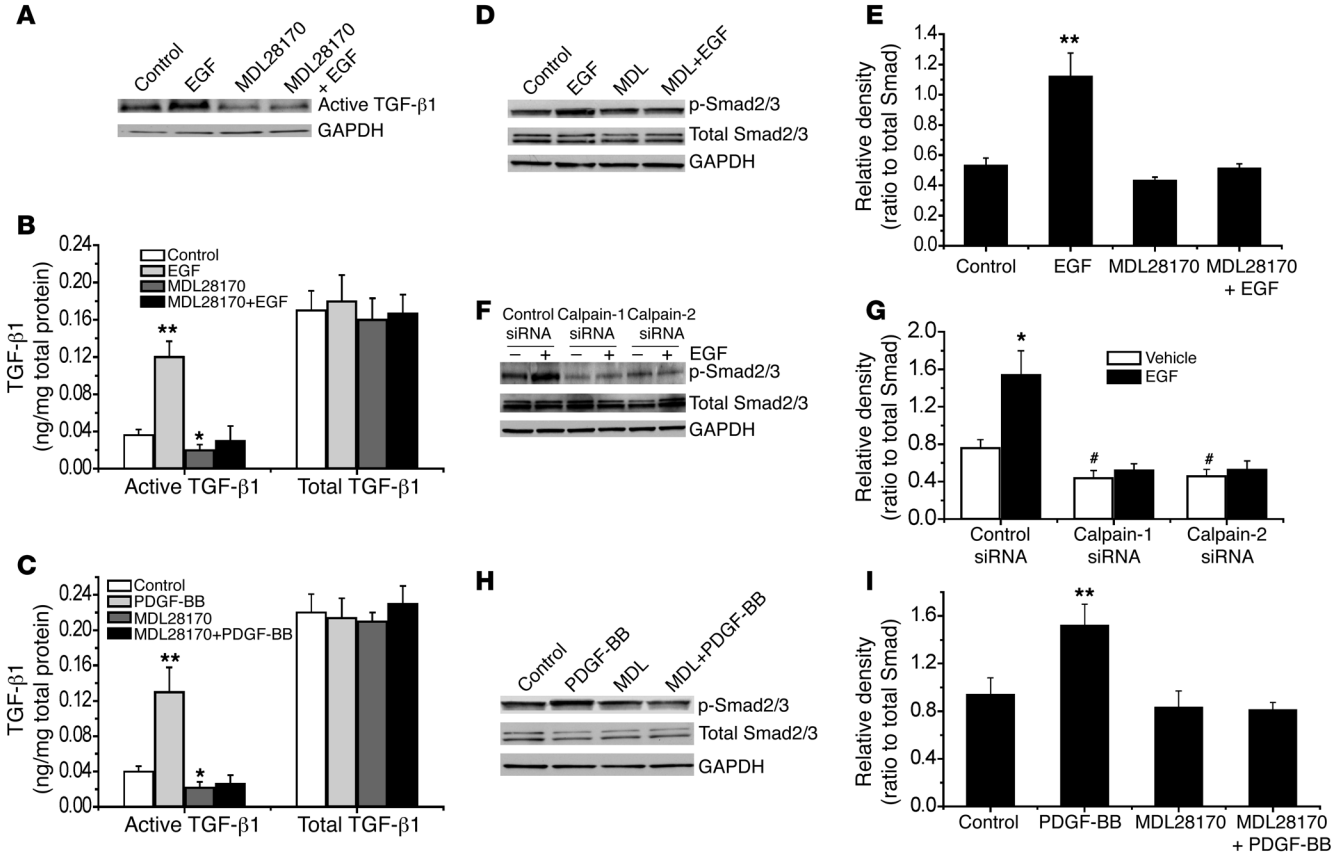

Figure 11

Inhibition of calpain blocks EGF- and PDGF-BB–induced increases in intracellular content of active TGF-β1 and p-Smad2/3 in PASMCs. PASMCs were incubated with EGF (10 ng/ml) or PDGF-BB (10 ng/ml) in the presence and absence of MDL28170 (20 μM) for 2 hours, after which the intracellular content of active TGF-β1 (**A**) and p-Smad2/3 (**D**, **E**, **H**, and **I**) was measured using Western blot analysis; intracellular active TGF-β1 content was also assayed using ELISA (**B** and **C**). (**F** and **G**) PASMCs were transfected with an siRNA against the mRNA of calpain-1 or calpain-2 or control (luciferase) siRNA. After 96 hours, the cells were incubated with EGF (10 ng/ml) for 2 hours, and then the protein content of p-Smad2/3 and total Smad2/3 was measured using immunoblotting. (**A**, **D**, **F**, and **H**) Representative immunoblots from 4 experiments. (**E**, **G**, and **I**) Changes in p-Smad2/3 and total Smad2/3 content quantified by scanning densitometry. Results are expressed as mean ± SEM; $n = 4$ experiments. $^{*}P < 0.05$, $^{**}P < 0.01$ versus control (without EGF or PDGF-BB). $^{\#}P < 0.05$ versus vehicle group in control siRNA. MDL, MDL28170.

TGF-β1 signaling pathway may play an important role in pulmonary vascular remodeling in hypoxia- and MCT-induced pulmonary hypertension. Indeed, the TGF-β1/Smad pathway is critical in the pathogenesis of pulmonary hypertension. It has been reported that the TGF-β1/Smad pathway is upregulated in MCT- and chronic hypoxia–induced pulmonary hypertension (6, 7) and patients with pulmonary arterial hypertension (16). Inhibition of TGF-β1 signaling prevents or attenuates pulmonary vascular remodeling and elevated right ventricular pressure in animal models (6, 17, 18).

We then determined whether intracellular TGF-β activation and signaling occur in vivo. We found that chronic hypoxia–induced pulmonary vascular remodeling and pulmonary hypertension were prevented by the cell-permeable Alk5 inhibitor SB431542 but not by the cell-impermeable neutralizing anti–TGF-β antibody. These results suggest that calpain-induced activation of intracellular TGF-β1 signaling mediates pulmonary vascular remodeling and pulmonary hypertension.

It has been reported that blockade of EGF and PDGF receptor causes PASMC apoptosis, which is associated with regression of medial hypertrophy (11, 13). However, calpain inhibition does not cause apoptosis of PASMC. Consistent with these findings, our results show that calpain inhibition prevents progression of but does not reverse MCT-induced pulmonary hypertension. These data suggest that the apoptotic signal pathway caused by blockade of EGF and PDGF receptor is not recapitulated by calpain inhibition.

Besides mediating collagen synthesis and cell proliferation induced by EGF and PDGF-BB, calpain may play multiple roles in pulmonary hypertension. We found that calpain participated in PDGF-BB–induced increases in CTGF and migration of PASMCs. Duffy et al. (55) reported that calpain inhibition decreases endothelin-1 levels and pulmonary hypertension after cardiopulmonary bypass with deep hypothermic circulatory arrest. Moreover, Tabata et al. (56) found that the calpain inhibitor calpeptin prevents bleomycin-induced pulmonary fibrosis in mice. Thus, CTGF, endothelin, and lung fibroblasts may also contribute to the mediating role of calpain in pulmonary vascular remodeling and pulmonary hypertension. Notably, calpain inhibition affects vascular constriction and relaxation of pulmonary arteries. For example, we have previously reported that calpain inhibitors decrease gene expression of eNOS (57).

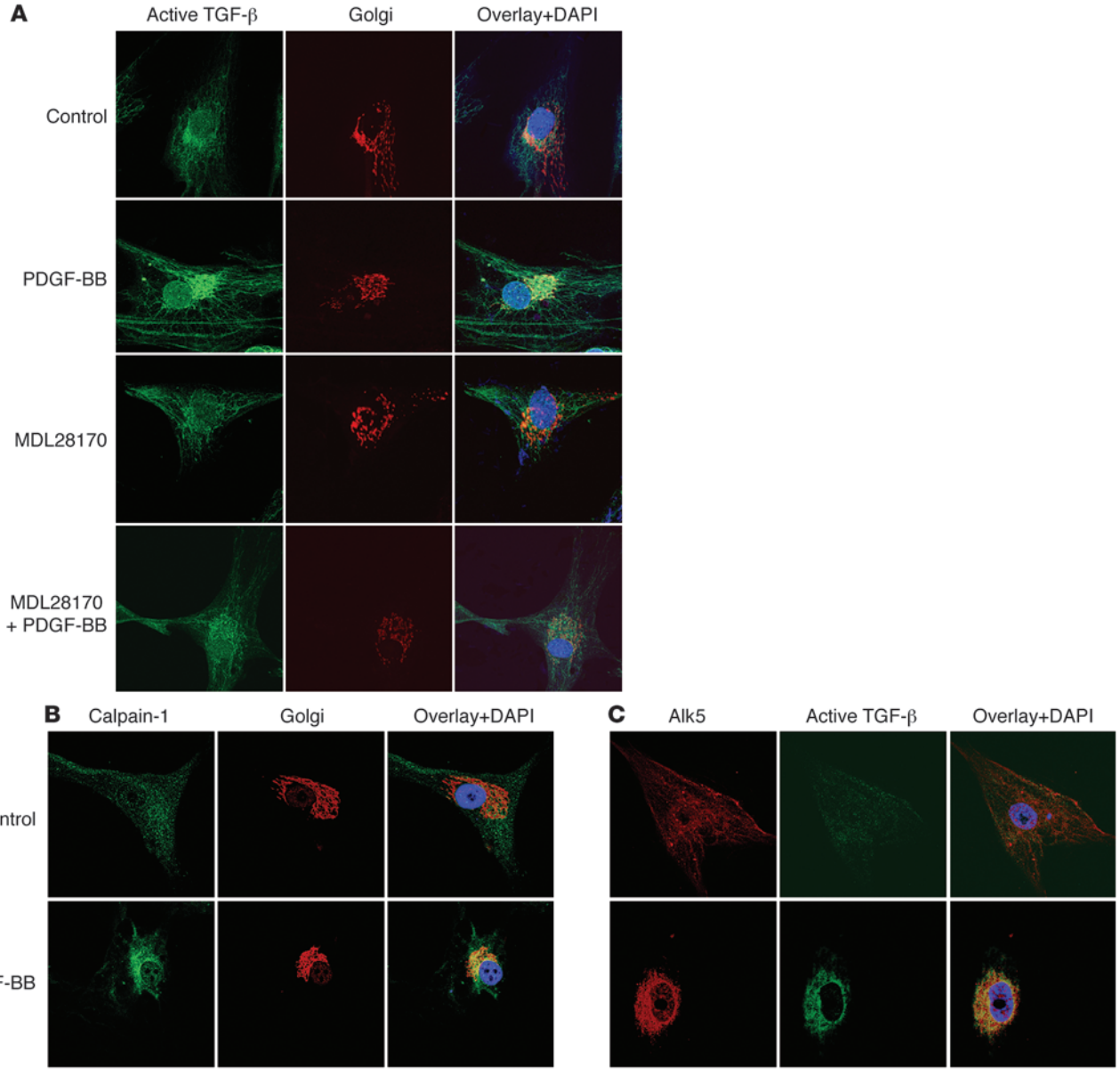

Figure 12
Colocalization of active TGF-β, Alk5, and calpain in the Golgi. (**A**) After treatment with or without the calpain inhibitor MDL28170 (20 μM) for 30 minutes, PASMCs were incubated with PDGF-BB (10 ng/ml) for another 30 minutes. Then the cells were double stained for Golgi (red) and active TGF-β (green) and counterstained by using DAPI (blue). (**B** and **C**) PASMCs were incubated with PDGF-BB (10 ng/ml) for 30 minutes and then double stained for Golgi (red) and calpain-1 (green) or Alk5 (red) and active TGF-β (green) and counterstained with DAPI (blue). Images are representative of 3 experiments. Original magnification, ×400.

Youn et al. (58) found that calpain inhibition decreases VEGF-induced eNOS phosphorylation at S1179. Although calpain can degrade HSP90 (59), an eNOS activator, endothelium-dependent vasorelaxation is reduced by calpain inhibitor (57) and calpain-4 knockout (Supplemental Figure 10). These data suggest that the combined effect of calpain is to help endothelium-dependent vasorelaxation. On the other hand, pulmonary arteries from calpain-4–knockout mice exhibit reduced contractility of smooth muscle, suggesting that calpain contributes to the processes of vasoconstriction, which may counteract endothelium-dependent vasorelaxation. Therefore, it is possible that vasoconstriction may contribute to the mediating role of calpain in pulmonary vascular remodeling and pulmonary hypertension. Further studies are needed to test this possibility.

We noted that inhibition of calpain using MDL28170 or calpain siRNAs causes a decrease in collagen synthesis in PASMCs, indicating that calpain helps maintain normal collagen synthesis of PASMCs. Nevertheless, conditional knockout of calpain and MDL28170 did not affect RVSP, wall thickness of pulmonary artery and right ventricle, or collagen I deposition in normal mice or rats. Our results showing that calpain inhibition prevents the progression of established pulmonary hyperten-

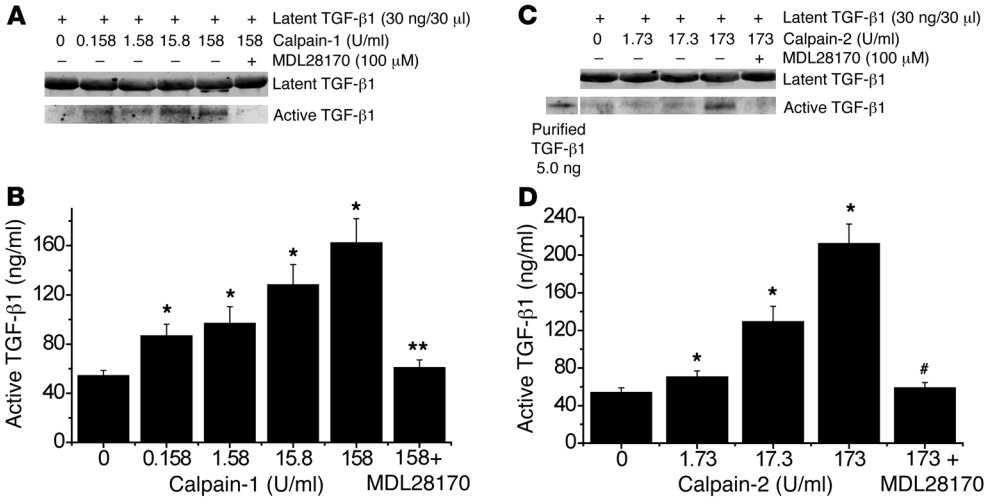

Figure 13

Calpain-1 and -2 activate latent TGF-β1 in vitro. (**A** and **C**) Purified latent TGF-β1 (30 ng/30 μl) was incubated with calpain-1 (0–158 U/ml) or calpain-2 (0–173 U/ml) in the presence of 5 mM calcium overnight at room temperature, after which the mixtures were subjected to Western blot analysis in non-denaturing and non-reducing conditions. (**B** and **D**) Active TGF-β1 in the mixture was also assayed using ELISA. Results are expressed as mean ± SEM; $n = 3$ experiments. $^{*}P < 0.05$ versus control (zero); $^{**}P < 0.05$ versus calpain-1 158 U/ml group; $^{\#}P < 0.05$ versus calpain-2 173 U/ml group.

sion without affecting pulmonary vascular function in normal rodents suggest that calpain is a promising therapeutic target for pulmonary hypertension.

Finally, we determined the level of calpain activation by measuring levels of the specific calpain cleavage product SBDP and of active TGF-β in smooth muscle of pulmonary arterioles of pulmonary hypertension patients. We observed increased calpain activity and active TGF-β in smooth muscle of pulmonary arterioles of pulmonary hypertension patients. These findings provide evidence that calpain in pulmonary vascular smooth muscle might be a novel target for intervention in pulmonary hypertension.

In summary, our findings provide evidence supporting the idea that calpain mediates EGF- and PDGF-induced collagen synthesis and proliferation of PASMCs via an intracrine TGF-β1 signaling pathway (Supplemental Figure 12). Calpain plays an important role in hypoxia- and MCT-induced pulmonary vascular remodeling and pulmonary hypertension.

Methods

Reagents and materials. Human PASMCs and culture medium were obtained from Lonza Walkersville Inc. EGF, VEGF, and PDGF-BB were obtained from Sigma-Aldrich. MDL28170, the fluorogenic peptide Suc-Leu-Leu-Val-Tyr-AMC, and purified calpain-1 and -2 were obtained from Calbiochem. Anti–collagen I antibody was obtained from Novus Biologicals. Anti–active TGF-β1 antibody, latent and active TGF-β1, and ELISA kit for EGF, TGF-β1, and PDGF-BB were obtained from R&D Systems (catalog numbers are indicated in the description of each experimental procedure). Antibodies against GAPDH were obtained from Cell Signaling Technology.

Conditional knockout of calpain-4. Because calpain-4 (small unit) is required for the activity of both calpain-1 and -2, deletion of calpain-4 prevents activation of both calpains. Targeted disruption of calpain-4 is embryonically lethal at days 10 and 11 as a result of severe defects in vascular development (60). Therefore, we took advantage of mice homozygous for floxed *Capn4* alleles (*Capn4*$^{fl/fl}$) (61) to create conditional knockout of calpain-4 in mice. *Capn4*$^{fl/fl}$ mice were crossed with B6.Cg-Tg (CAG-cre/Esr1)5Amc/J mice (The Jackson Laboratory) to generate *ER-Cre*$^{+/-}$ *Capn4*$^{fl/+}$ mice. These mice were then crossed with either *Capn4*$^{fl/fl}$ or *Capn4*$^{fl/+}$ mice to generate *ER-Cre*$^{+/-}$ *Capn4*$^{fl/fl}$ mice. PCR and Southern blot analysis were used to genotype these mice. Deletion of calpain-4 was induced by administration of tamoxifen (20 mg/kg/d, i.p.) for 5 days and was confirmed by analysis of calpain-4 using Western blotting (Figure 1), fluorescence confocal microscopy (Supplemental Figure 1), and Southern blotting (Supplemental Figure 2) of lung tissues. Control mice were littermate *Capn4*$^{fl/fl}$ or *Capn4*$^{fl/+}$ mice treated with the same tamoxifen regimen. Mice between 12 and 16 weeks of age were used for the hypoxic pulmonary hypertension model.

Hypoxic pulmonary hypertension model in mice. Five days after a regimen of tamoxifen administration, control and *ER-Cre*$^{+/-}$*Capn4*$^{fl/fl}$ mice were exposed to room air (normoxia) or 10% oxygen (hypoxia) in a clear plastic polypropylene chamber (30 × 20 × 20 in.). The oxygen concentration (10%) was maintained using ProOx Oxygen Controller (BioSpherix). The chamber has ventilation holes and a small, quiet fan to provide forced circulation and instant homogenization of gases. Litholyme CO_2 absorbent (Allied Healthcare Products) kept the CO_2 concentration at less than 0.2%. Boric acid was used to maintain minimal NH_3 levels within the chamber. Relative humidity within the chamber was kept at less than 60% with anhydrous $CaSO_4$. All animals had access to standard mouse chow and water ad libitum under both normoxic and hypoxic conditions. After 3 weeks, pulmonary hypertension and pulmonary vascular remodeling were assessed.

In another experiment, male C57BL/6 mice at 12 weeks of age were exposed to normoxia or hypoxia as described above. At the beginning of the second week, groups of normoxic and hypoxic mice were injected with neutralizing anti–TGF-β antibody (R&D Systems, AB-100-NA; 10 mg/kg, i.p, twice a week) (62) or SB431542 (4.2 mg/kg, i.p., daily) (63). The doses of neutralizing anti–TGF-β antibody and SB431542 were chosen according to previous reports (62, 63). Three weeks after hypoxia, pulmonary hypertension and pulmonary vascular remodeling were assessed. For measurement of plasma TGF-β1 levels, blood was drawn through the right ventricle after thoracotomy using a syringe rinsed with heparin (160 U/ml). 0.8 ml of blood was then mixed with 0.1 ml of heparin (160 U/ml) on ice. The blood was immediately centrifuged at 1,000 *g* for 20 minutes at 4°C. The supernatant was centrifuged again at 10,000 *g* for 10 minutes at 4°C to completely remove platelets. The plasma preparations were stored at –80°C. Active TGF-β1 levels in plasma were determined using ELISA kits from R&D Systems (MB100B). A standard curve was made using standard recombinant TGF-β1 from 31.2 to 1,000 pg/ml. The minimum detectable dose of TGF-β1 ranged from 1.7 to 15.4 pg/ml according to the manufacturer's instructions, and we could detect TGF-β1 as low as 4.0 pg/ml. The remaining procedures were performed according to manufacturer's instructions.

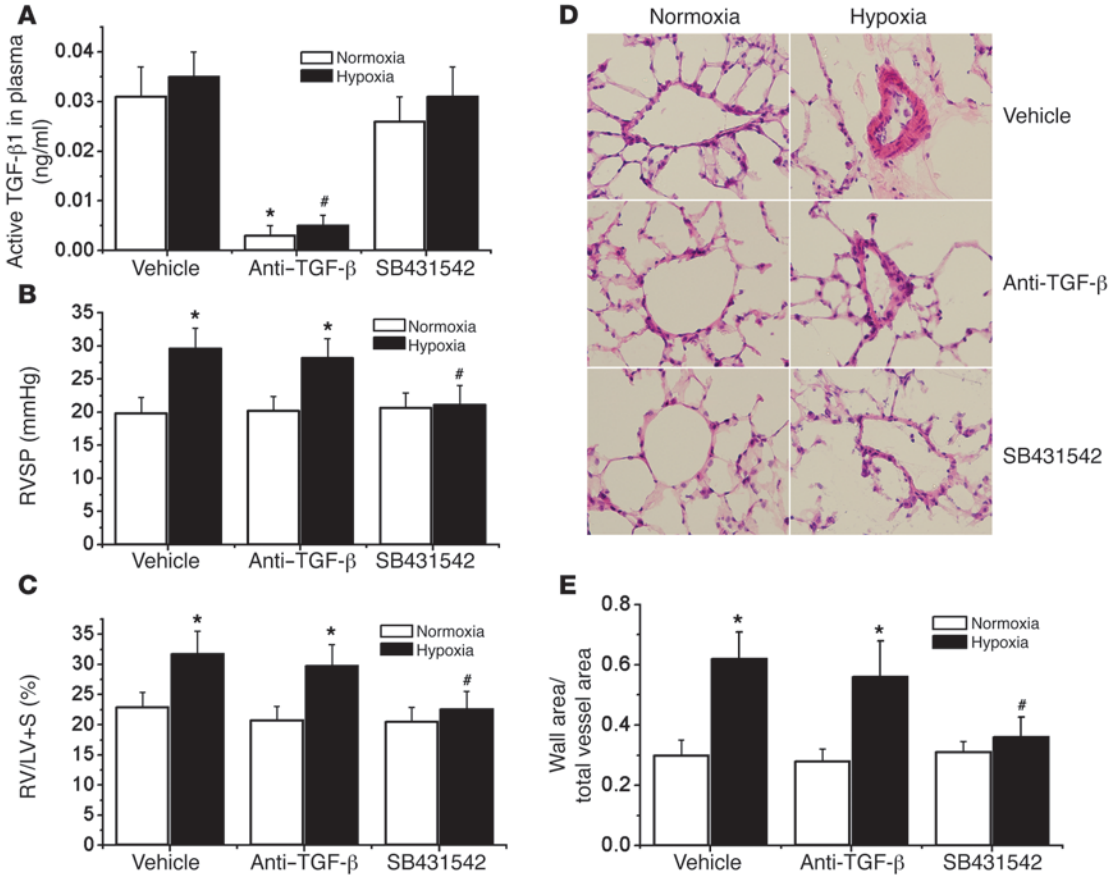

Figure 14

Effects of neutralizing anti–TGF-β antibody and Alk5 inhibitor SB431542 on chronic hypoxia–induced pulmonary hypertension and pulmonary vascular remodeling. Mice were exposed to room air (normoxia) or 10% oxygen (hypoxia). At the beginning of second week, groups of normoxic and hypoxic mice were injected with neutralizing anti–TGF-β antibody (10 mg/kg, i.p., twice a week) or SB431542 (4.2 mg/kg, i.p., daily). Three weeks after hypoxia, plasma TGF-β1 levels, pulmonary hypertension, and pulmonary vascular remodeling were assessed. (**A**) Changes in active TGF-β1 levels in plasma. (**B**) Changes in RVSP. (**C**) Changes in RV/LV+S. (**D**) Representative images of lung sections of normoxic or hypoxic mice with or without neutralizing anti–TGF-β antibody and SB431542. Original magnification, ×400. (**E**) Changes in ratio of wall area to total vessel area in the lung sections. Results are expressed as mean ± SEM; $n = 6$. $^{*}P < 0.05$ versus normoxia; $^{\#}P < 0.05$ versus hypoxia group with vehicle.

MCT-induced pulmonary hypertension in rats. Male Sprague-Dawley rats 8 weeks of age were purchased from Charles River. Pulmonary hypertension was induced by a single subcutaneous injection of MCT (60 mg/kg). Control rats received saline (0.5 ml, subcutaneously). After 2 weeks, pulmonary hypertension and pulmonary vascular remodeling were determined in 6 control rats and 6 MCT-injected rats. At the beginning of the third week after MCT treatment, another 6 control rats and 6 MCT-injected rats started to receive the calpain inhibitor MDL28170 (20 mg/kg, i.p.) once daily. This dose was chosen based on prior experiments (64). In addition, a second group of MCT-injected rats ($n = 6$) received the same volume of vehicle (0.2 ml DMSO, i.p.). Pulmonary hypertension and pulmonary vascular remodeling were assessed at the end of the third week after MCT injection.

Assessment of pulmonary hypertension. Mice were anesthetized (pentobarbital, 90 mg/kg, i.p.), and the trachea was intubated. The right external jugular vein was surgically exposed and cannulated with a 1.4-F microtip pressure transducer catheter (Millar Instruments). The transducer was advanced into the right ventricle, and right ventricular pressure was continuously monitored for 10 minutes. Heart rates (300–450 beats/min were deemed acceptable) and pressure waveforms were monitored to ensure the validity of the pressure measurements. Data were recorded using a PowerLab data acquisition system (ADInstruments). These measurements were made 2 hours after hypoxia.

Rats were anesthetized (pentobarbital, 50 mg/kg, i.p.) and the trachea intubated. The right external jugular vein was surgically exposed and cannulated with a catheter connected to a pressure transducer (ADInstruments). The catheter was advanced into the right ventricle, and right ventricular pressure was continuously monitored for 10 minutes. Data were recorded using a PowerLab data acquisition system.

Histological analysis. After hemodynamic measurements, the mice and rats were euthanized by thoracotomy. The blood in pulmonary circulation was rinsed by infusing PBS through the pulmonary artery, and the heart and lungs were removed. The free wall of the right ventricle (RV), left ventricle (LV), and septum (S) were then carefully dissected and individually weighed to calculate the ratio RV/LV+S as an index of right ventricular hypertrophy.

The right lungs were removed and snap frozen in liquid nitrogen for preparation of homogenates, and the left lungs were filled with 4% PFA solution with 0.5% agarose at 25 cm H_2O and fixed in 4% PFA for 24 hours. The fixed lungs were then sliced mid-sagittally and embedded in paraffin. The slides (7 μm thickness) were stained with hematoxylin and

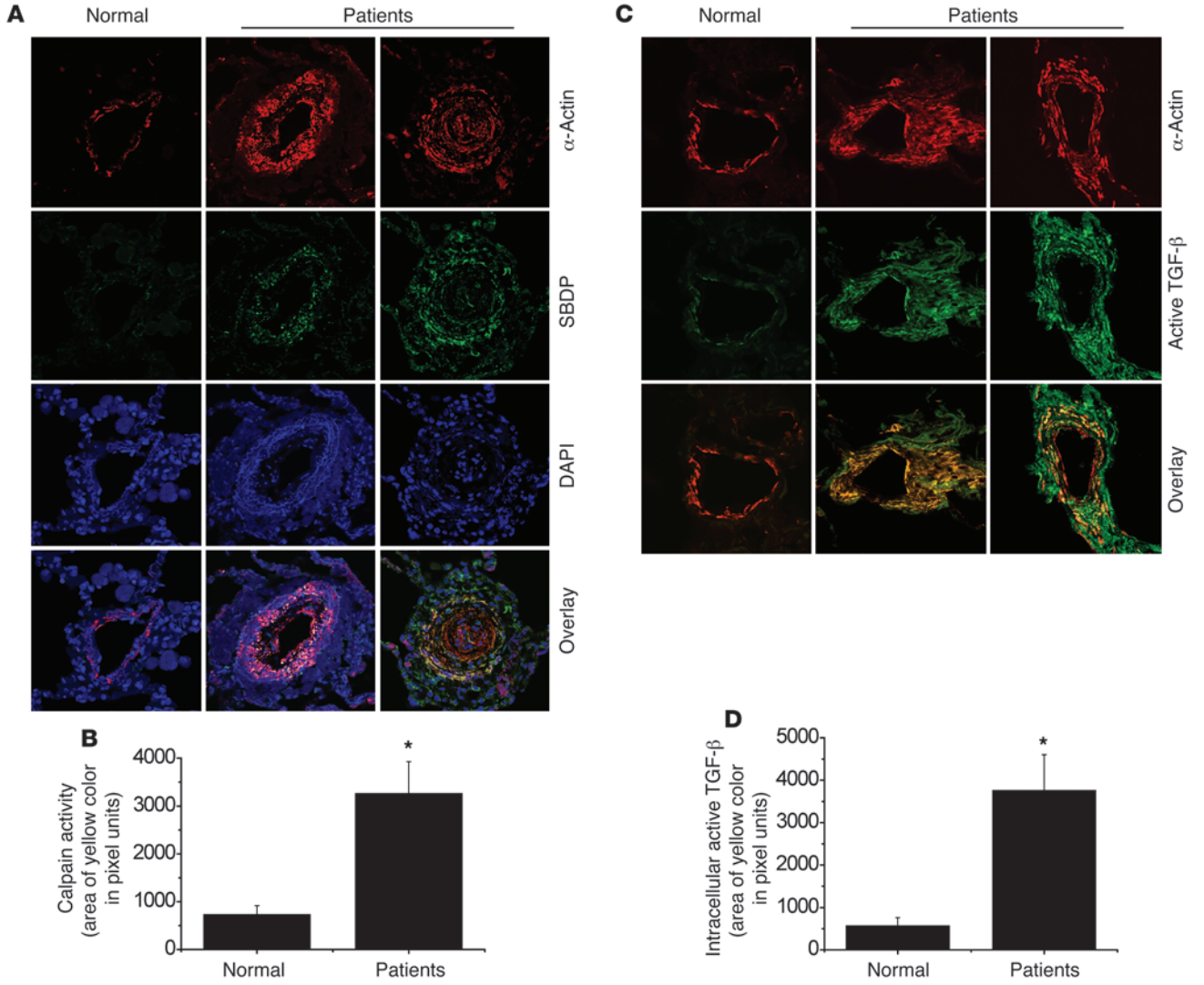

Figure 15

Levels of calpain activation and active TGF-β in smooth muscle cells of muscular pulmonary arteries of patients with pulmonary arterial hypertension. (**A** and **C**) Higher level of calpain activation and active TGF-β in smooth muscle of pulmonary arterioles of patients with pulmonary arterial hypertension. Human lung slides were double stained for α-actin (red), SBDP (green), or active TGF-β (green) and counterstained by using DAPI (blue). Images are representative of lung tissues from patients with idiopathic pulmonary arterial hypertension ($n = 6$) and normal lungs ($n = 5$). Original magnification, ×400. (**B** and **D**) Changes in calpain activity and intracellular active TGF-β in smooth muscle of pulmonary arterioles. *$P < 0.05$ versus normal. Results are expressed as mean ± SEM.

eosin for morphometric analysis and were examined with an Olympus BX41 microscope. An Olympus DP72 digital camera and ImageJ software (http://rsbweb.nih.gov/ij/) were used to analyze slides. A minimum of 10 microscopic fields were examined for each slide. To quantitate pulmonary arterial wall thickness, the lumen area at the level of the basement membrane and total vascular area at the adventitial border in 20 muscular arteries with diameter of 50–100 μm per lung section were outlined, and area sizes were measured using ImageJ. The vascular wall thickness was calculated as follows: wall thickness = (total vascular area − lumen area)/total vascular area.

To determine the extent of collagen deposition in pulmonary arterioles, double immunostaining of collagen I/α-actin was performed. The lung slides were incubated first with a goat polyclonal antibody against collagen I (dilution 1:50, Novus Biologicals) and mouse monoclonal antibody against α-actin (dilution 1:700, Santa Cruz Biotechnology Inc.) overnight and then with donkey anti-goat IgG–Alexa Fluor 488 and goat anti-mouse IgG–Alexa Fluor 594 (dilution 1:500, Invitrogen). The slides were sealed with mounting solution containing antifade reagent and were examined using a Zeiss LSM 510 laser scanning confocal microscope.

Measurement of calpain activation in lung tissues. To measure the level of calpain activation in pulmonary arterioles, SBDP was detected as described previously (65, 66). Spectrin contains a specific calpain cleavage site and releases SBDP (67), which can be detected by antibody. This is a widely accepted method to detect calpain activation in vivo (65, 66, 68). Lung slides of 7-μm thickness were incubated first with a rabbit polyclonal antibody against SBDP (developed by our laboratory) and mouse monoclonal antibody against α-actin overnight and then with goat anti-rabbit IgG–Alexa Fluor 488 and goat anti-mouse IgG–Alexa

Fluor 594. The slides were sealed with mounting solution containing antifade reagent and DAPI and were examined using a Zeiss LSM 510 laser scanning confocal microscope.

Protein analyses in lung tissues. Protein levels of calpain-1, calpain-2, calpain-4, calpastatin, collagen-1, Smad, and GAPDH in lung homogenates were measured using Western blot analysis. The lung tissues were homogenated in RIPA buffer and mixed with Western blot sample buffer. Samples (10–30 μg protein) were denatured and electrophoresed on SDS-PAGE gel. Separated proteins were electrotransferred to nitrocellulose membranes, incubated with 1% BSA for 1 hour, and then incubated with monoclonal antibodies against calpain-1 (dilution 1:5,000, Triple Point Biologics), calpain-2 (dilution 1:5,000, Triple Point Biologics), calpain-4, calpastatin (dilution 1:1,000, Sigma-Aldrich), collagen I (dilution 1:1,000, Novus Biologicals), phospho-Smad2/3 (dilution 1:100, Santa Cruz Biotechnology Inc.), total Smad2/3 (dilution 1:1,000, Cell Signaling Technology), and GAPDH (dilution 1:5,000, Cell Signaling Technology) overnight at 4°C and then washed with 50 ml of 0.1% Tween 20, 20 mm Tris-HCl (pH 7.5), and 150 mm NaCl (TTBS) 3 times for 10 minutes. Secondary antibody IgG conjugated to alkaline phosphatase (Bio-Rad) was diluted in TTBS plus 1% BSA and incubated with the membranes at room temperature for 1 hour. After the membranes were washed with TTBS, enhanced chemiluminescence (Immun-Star, Bio-Rad) was used to visualize the reactive proteins, followed by densitometric quantification using ImageJ.

Active TGF-β1, total TGF-β1, EGF, and PDGF-BB in lung homogenates were measured using ELISA kits from R&D Systems (MB100B, MEG00, MBB00). Snap-frozen lung tissues were homogenized using a BulletBlender tissue homogenizer (Next Advance) after thawing in PBS containing protease inhibitors (1 protease inhibitor cocktail tablet per 10 ml buffer, 11836170001, Roche Applied Science). The homogenates were centrifuged at 10,000 *g* for 30 minutes at 4°C. The supernatants were used in assays of TGF-β1, EGF, and PDGF-BB without further freezing/thawing. The TGF-β1 assay only measures biologically active TGF-β1. One aliquot was assayed to detect total TGF-β1 by incubating with 1 N HCl to activate latent TGF-β1; the other aliquot was assayed without adding 1 N HCl for detection of active TGF-β1. A standard curve was made using standard recombinant TGF-β1 from 31.2 to 1,000 pg/ml. The minimum detectable dose of TGF-β1 ranged from 1.7 to 15.4 pg/ml according to the manufacturer's instructions; we were able to detect TGF-β1 as low as 4.0 pg/ml. The concentrations of active TGF-β1 in undiluted supernatant without adding 1 N HCl ranged from 46 to 117 pg/ml. The total protein levels were measured using a Pierce BCA assay kit from Fisher Scientific (catalog 23225). The normalized TGF-β1 concentrations (ng/mg protein) were calculated by dividing TGF-β1 concentrations (ng/ml) by total protein concentration (mg/ml). The remaining procedures were performed according to the manufacturer's instructions.

Intracellular calpain activation and active TGF-β in human lung samples. Human lung slides were obtained from lung tissues of patients undergoing lung transplantation for idiopathic pulmonary arterial hypertension ($n = 6$) and from unused donor lungs (normal lungs, $n = 5$). These samples were provided by the University of Colorado Denver and the Pulmonary Hypertension Breakthrough Initiative (PHBI). To measure the level of calpain activation in pulmonary arterioles, the specific calpain cleavage product SBDP was detected as described above. The slides were double labeled for SBDP and α-actin and counterstained using DAPI. Intracellular active TGF-β was stained using cryosectioned slides and anti–TGF-β antibody (R&D Systems, MAB1835, clone 1D11), which specifically detects the biologically active TGF-β. This method has been widely used to stain active TGF-β in tissues (36, 69–71). The fluorescence-labeled slides were examined using a Zeiss LSM 510 laser scanning confocal microscope. The yellow color indicates colocalization of SBDP and α-actin or intracellular active TGF-β and α-actin. The area of yellow color was measured using ImageJ.

Cell culture. Human PASMCs were purchased from Lonza and cultured according to the supplier's instructions. Third- to eighth-passage cells equilibrated in growth factor–free medium for 24 hours were used for all experiments.

Measurement of calpain activity in PASMCs. Calpain activity in PASMC was measured using the fluorogenic peptide Suc-Leu-Leu-Val-Tyr-AMC as a substrate following a procedure described previously (72) with slight modification. Briefly, cells were cultured in 24-well plates. After being washed twice with PBS, Suc-Leu-Leu-Val-Tyr-AMC was added to a final concentration of 80 μM in growth factor–free medium in the presence and absence of MDL28170. Immediately after the addition of Suc-Leu-Leu-Val-Tyr-AMC, fluorescence was recorded at 2-minute intervals for 20 minutes at excitation 360 nm and emission 460 nm using a SpectraMax M2e microplate reader (Molecular Devices). Calpain activity was expressed as fluorescence units in the absence of MDL28170 subtracted by fluorescence units in the presence of MDL28170.

Cell proliferation assay. Proliferation of PASMCs was assayed with a kit from Roche that monitors the incorporation of BrdU into newly synthesized DNA. BrdU was detected using anti-BrdU–peroxidase conjugate in accordance with the manufacturer's instructions. After the reactions were stopped, absorbance at 450 nm was measured by using a SpectraMax M2e microplate reader.

Determination of COL1A1 mRNA. After treatment, total RNA of PASMCs was extracted by using an RNeasy Mini kit from QIAGEN according to the manufacturer's protocol. To measure *COL1A1* mRNA, quantitative real-time RT-PCR was performed using TaqMan gene expression assay from Applied Biosystems (assay ID: Hs00164004_m1 for human *COL1A1*; primer sequences have not been disclosed by the company). ABI 7500 Sequence Detector (PerkinElmer Applied Biosystems) was programmed for the PCR conditions: 95°C for 10 minutes, 40 cycles of 95°C for 15 seconds, and 60°C for 1 minute. *COL1A1* mRNA content was expressed as $2^{-\Delta\Delta CT}$ using 18s rRNA as a reference.

siRNA knockdown of calpain-1 and calpain-2. Expression of calpain-1 and calpain-2 was silenced using siRNA technology (73). The target sequences for the mRNA of calpain-1 and calpain-2 were 5′-AAGCTAGTGTTCGTGCACTCT-3′ and 5′-AAACCAGAGCTTCCAGGAAAA-3′, respectively. The siRNA against luciferase mRNA was used as a control siRNA with a target sequence of 5′-AACGTACGCGGAATACTTCGA-3′. The calpain and luciferase siRNAs were custom synthesized by QIAGEN. All siRNAs were transfected into PASMCs using QIAGEN RNAiFect transfection reagent in accordance with the manufacturer's instructions. Three days after transfection, the medium was changed to serum-free medium. Levels of calpain-1, calpain-2, and other proteins were determined after 96 hours.

Activation of latent TGF-β1 by calpain in vitro. Purified latent TGF-β1 (R&D Systems, 299-LT/CF, final concentration, 1.0 ng/μl) was incubated with purified calpain-1 (Calbiochem, 208712, 0-158 U/ml) or calpain-2 (Calbiochem, 208718, 0-173 U/ml) in 200 μl DMEM medium containing 5 mM calcium at room temperature overnight, after which the mixtures were subjected to Western blot analysis in non-denaturing and non-reducing conditions. 30 μl of mixture was mixed with 8 μl of native sample buffer (Bio-Rad, 161-0738) and then directly loaded onto a Tris-Tricine precast gel (Bio-Rad, 345-0067). After transfer, latent and active TGF-β1 were detected on the membranes using anti–TGF-β1 antibody (R&D Systems, MAB240) as previously reported (74). In the meantime, the identity of the band for the putative active TGF-β1 was verified by mass spectrometry. Active TGF-β1 in the mixture was also assayed using ELISA kits from R&D Systems (DB100B) as described above.

Confocal microscopy of PASMCs. To determine the intracellular localization of active TGF-β, Alk5, and calpain, PASMCs were incubated with PDGF-BB (10 ng/ml) for 30 minutes. Then cells were double stained using antibodies

against Golgi (Abcam, Ab52649) and active TGF-β (R&D Systems, MAB1835, clone 1D11), Alk5 (Santa Cruz Biotechnology Inc., SC-398) and active TGF-β, or Golgi and calpain-1 (Enzo Life Sciences, ALX-804-050). The fluorescence-labeled cells were examined using a Zeiss LSM 510 laser scanning confocal microscope.

Assay of PASMC migration. Migration assays were performed using a Boyden chamber (Neuroprobe) as described previously (75). PASMCs were digested with 0.05% trypsin and dispersed into homogeneous cell suspensions that were placed in the upper chamber of a 48-well Boyden chamber in the presence or absence of PDGF-BB (10 ng/ml) or MDL28170 (20 μM) in both upper and lower chambers. The cells were allowed to migrate for 4 hours. Cells that migrated to the lower sides of the filter membranes were fixed and subjected to hematoxylin and eosin staining. The results are expressed as the number of migrated cells per square millimeter.

Apoptosis assay. Apoptosis of PASMCs treated with PDGF-BB or MDL28170 for 24 hours was evaluated by flow cytometric analysis of apoptotic cells for active caspase-3 using an FITC Active Caspase-3 Apoptosis Kit (BD Biosciences — Pharmingen, 550480). PASMCs treated with 3 mM H_2O_2 were used as positive control.

Determination of endothelium-dependent vasorelaxation, smooth muscle contractility, and reactivity to NO. Main pulmonary arteries were isolated from calpain-4–knockout mice and control mice and cleaned and cut into 1.5-mm rings. The pulmonary artery rings were mounted under a resting tension of 5.0 mN in a myograph organ bath chambers (Danish Myo Technology A/S) filled with Krebs solution at 37°C (pH 7.4) and continuously bubbled with a mixture of 95% O_2 and 5% CO_2. Isometric force was recorded using a PowerLab/8SP data acquisition system (ADInstruments). The tissues were allowed to equilibrate for 1 hour before starting the experiments. After equilibration, pulmonary artery rings were contracted with high-KCl solution (80 mM) to verify the viability of the preparations. After washing out the KCl, cumulative concentration-response curves to acetylcholine (0.001–10 μM) were obtained after pre-contraction with phenylephrine (1 μM). The endothelium-dependent vasorelaxation was expressed as a percentage of phenylephrine contraction. In another set of experiments, cumulative concentration-response curves to sodium nitroprusside (SNP; 0.0001–1 μM) or phenylephrine (0.001–10 μM) were also performed in endothelium-denuded pulmonary artery rings from control and calpain-4–knockout mice. Smooth muscle contractility was expressed as a percentage of KCl contraction. The reactivity to NO was expressed as a percentage of phenylephrine contraction.

Statistics. Results are shown as the mean ± SEM for *n* experiments. One-way ANOVA and *t* test analysis (2-tailed) were used to determine the significance of differences between the means of different groups. A *P* value less than 0.05 was considered statistically significant.

Study approval. All animal experiments were performed in accordance with the guiding principles of the NIH *Guide for the Care and Use of Laboratory Animals* and approved by the IACUC of the Georgia Health Sciences University. In the studies of human lung samples, patient identifiers including name, age, sex, and ethnic group were concealed. Waiver of informed consent was approved by the Human Assurance Committee (HAC) of the Georgia Health Sciences University and Institutional Review Board (COMIRB) of the University of Colorado and by PHBI.

Acknowledgments

We thank the PHBI for providing some of the human lung slides and Lisa Palmer at the University of Virginia Health System at Charlottesville for technical assistance. This work was supported by NIH grant R01HL088261 (to Y. Su), Flight Attendants Medical Research Institute grant 072104 (to Y. Su), American Heart Association Greater Southeast Affiliate grant 0855338E (to Y. Su), Medical College of Georgia Cardiovascular Discovery Institute grant (to Y. Su), and Canadian Institutes of Health Research grant MOP-81189 (to P.A. Greer).

Received for publication February 24, 2011, and accepted in revised form August 25, 2011.

Address correspondence to: Yunchao Su, Department of Pharmacology and Toxicology, Medical College of Georgia, Georgia Health Sciences University, 1120 15th Street, Augusta, Georgia 30912, USA. Phone: 706.721.7641; Fax: 706.721.2347; E-mail: ysu@georgiahealth.edu.

1. Tuder RM. Pathology of pulmonary arterial hypertension. *Semin Respir Crit Care Med*. 2009; 30(4):376–385.
2. Rabinovitch M. Molecular pathogenesis of pulmonary arterial hypertension. *J Clin Invest*. 2008; 118(7):2372–2379.
3. Stenmark KR, Meyrick B, Galie N, Mooi WJ, McMurtry IF. Animal models of pulmonary arterial hypertension: the hope for etiological discovery and pharmacological cure. *Am J Physiol Lung Cell Mol Physiol*. 2009;297(6):L1013–L1032.
4. Rabinovitch M. Pathobiology of pulmonary hypertension. *Annu Rev Pathol*. 2007;2:369–399.
5. Hassoun PM, et al. Inflammation, growth factors, and pulmonary vascular remodeling. *J Am Coll Cardiol*. 2009;54(1 suppl):S10–S19.
6. Long L, et al. Altered bone morphogenetic protein and transforming growth factor-beta signaling in rat models of pulmonary hypertension: potential for activin receptor-like kinase-5 inhibition in prevention and progression of disease. *Circulation*. 2009;119(4):566–576.
7. Arcot SS, Lipke DW, Gillespie MN, Olson JW. Alterations of growth factor transcripts in rat lungs during development of monocrotaline-induced pulmonary hypertension. *Biochem Pharmacol*. 1993; 46(6):1086–1091.
8. Gillespie MN, et al. Polyamines and epidermal growth factor in monocrotaline-induced pulmonary hypertension. *Am Rev Respir Dis*. 1989; 140(5):1463–1466.
9. Jones PL, Cowan KN, Rabinovitch M. Tenascin-C, proliferation and subendothelial fibronectin in progressive pulmonary vascular disease. *Am J Pathol*. 1997;150(4):1349–1360.
10. Sheng L, Zhou W, Hislop AA, Ibe BO, Longo LD, Raj JU. Role of epidermal growth factor receptor in ovine fetal pulmonary vascular remodeling following exposure to high altitude long-term hypoxia. *High Alt Med Biol*. 2009;10(4):365–372.
11. Merklinger SL, Jones PL, Martinez EC, Rabinovitch M. Epidermal growth factor receptor blockade mediates smooth muscle cell apoptosis and improves survival in rats with pulmonary hypertension. *Circulation*. 2005;112(3):423–431.
12. Selimovic N, Bergh CH, Andersson B, Sakiniene E, Carlsten H, Rundqvist B. Growth factors and interleukin-6 across the lung circulation in pulmonary hypertension. *Eur Respir J*. 2009;34(3):662–668.
13. Schermuly RT, et al. Reversal of experimental pulmonary hypertension by PDGF inhibition. *J Clin Invest*. 2005;115(10):2811–2821.
14. Ziino AJ, et al. Effects of rho-kinase inhibition on pulmonary hypertension, lung growth, and structure in neonatal rats chronically exposed to hypoxia. *Pediatr Res*. 2010;67(2):177–182.
15. Nisbet RE, et al. Rosiglitazone attenuates chronic hypoxia-induced pulmonary hypertension in a mouse model. *Am J Respir Cell Mol Biol*. 2010; 42(4):482–490.
16. Thomas M, et al. Activin-like kinase 5 (ALK5) mediates abnormal proliferation of vascular smooth muscle cells from patients with familial pulmonary arterial hypertension and is involved in the progression of experimental pulmonary arterial hypertension induced by monocrotaline. *Am J Pathol*. 2009;174(2):380–389.
17. Zaiman AL, et al. Role of the TGF-beta/Alk5 signaling pathway in monocrotaline-induced pulmonary hypertension. *Am J Respir Crit Care Med*. 2008; 177(8):896–905.
18. Chen YF, et al. Dominant negative mutation of the TGF-beta receptor blocks hypoxia-induced pulmonary vascular remodeling. *J Appl Physiol*. 2006; 100(2):564–571.
19. Richter A, Yeager ME, Zaiman A, Cool CD, Voelkel NF, Tuder RM. Impaired transforming growth factor-beta signaling in idiopathic pulmonary arterial hypertension. *Am J Respir Crit Care Med*. 2004; 170(12):1340–1348.
20. Goll DE, Thompson VF, Li H, Wei W, Cong J. The calpain system. *Physiol Rev*. 2003;83(3):731–801.
21. Perrin BJ, Huttenlocher A. Calpain. *Int J Biochem Cell Biol*. 2002;34(7):722–725.
22. Suzuki K, Hata S, Kawabata Y, Sorimachi H. Structure, activation, and biology of calpain. *Diabetes*. 2004;53 suppl 1:S12–S18.
23. Suzuki K, Sorimachi H, Yoshizawa T, Kinbara K, Ishiura S. Calpain: novel family members, activation, and physiologic function. *Biol Chem Hoppe*

Seyler. 1995;376(9):523–529.
24. Sorimachi H, Suzuki K. The structure of calpain. *J Biochem (Tokyo)*. 2001;129(5):653–664.
25. Xu Y, Mellgren RL. Calpain inhibition decreases the growth rate of mammalian cell colonies. *J Biol Chem*. 2002;277(24):21474–21479.
26. Wendt A, Thompson VF, Goll DE. Interaction of calpastatin with calpain: a review. *Biol Chem*. 2004; 385(6):465–472.
27. Glading A, Lauffenburger DA, Wells A. Cutting to the chase: calpain proteases in cell motility. *Trends Cell Biol*. 2002;12(1):46–54.
28. Arora AS, de Groen PC, Croall DE, Emori Y, Gores GJ. Hepatocellular carcinoma cells resist necrosis during anoxia by preventing phospholipase-mediated calpain activation. *J Cell Physiol*. 1996; 167(3):434–442.
29. Grozio A, Catassi A, Cavalieri Z, Paleari L, Cesario A, Russo P. Nicotine, lung and cancer. *Anticancer Agents Med Chem*. 2007;7(4):461–466.
30. Qiu K, Su Y, Block ER. Use of recombinant calpain–2 siRNA adenovirus to assess calpain–2 modulation of lung endothelial cell migration and proliferation. *Mol Cell Biochem*. 2006;292(1–2):69–78.
31. Barnoy S, Maki M, Kosower NS. Overexpression of calpastatin inhibits L8 myoblast fusion. *Biochem Biophys Res Commun*. 2005;332(3):697–701.
32. Franco SJ, Huttenlocher A. Regulating cell migration: calpains make the cut. *J Cell Sci*. 2005; 118(pt 17):3829–3838.
33. Glading A, Uberall F, Keyse SM, Lauffenburger DA, Wells A. Membrane proximal ERK signaling is required for M-calpain activation downstream of epidermal growth factor receptor signaling. *J Biol Chem*. 2001;276(26):23341–23348.
34. Ji QS, Carpenter G. Role of basal calcium in the EGF activation of MAP kinases. *Oncogene*. 2000; 19(14):1853–1856.
35. Estacion M, Mordan LJ. PDGF-stimulated calcium influx changes during in vitro cell transformation. *Cell Signal*. 1997;9(5):363–366.
36. Gressner OA, et al. Activation of TGF-beta within cultured hepatocytes and in liver injury leads to intracrine signaling with expression of connective tissue growth factor. *J Cell Mol Med*. 2008; 12(6B):2717–2730.
37. Ambalavanan N, Li P, Bulger A, Murphy-Ullrich J, Oparil S, Chen YF. Endothelin-1 mediates hypoxia-induced increases in vascular collagen in the newborn mouse lung. *Pediatr Res*. 2007;61(5 Pt 1):559–564.
38. Yamataka T, Puri P. Active collagen synthesis by pulmonary arteries in pulmonary hypertension complicated by congenital diaphragmatic hernia. *J Pediatr Surg*. 1997;32(5):682–687.
39. Tozzi CA, Christiansen DL, Poiani GJ, Riley DJ. Excess collagen in hypertensive pulmonary arteries decreases vascular distensibility. *Am J Respir Crit Care Med*. 1994;149(5):1317–1326.
40. Stenmark KR, Fagan KA, Frid MG. Hypoxia-induced pulmonary vascular remodeling: cellular and molecular mechanisms. *Circ Res*. 2006; 99(7):675–691.
41. Humbert M, et al. Cellular and molecular pathobiology of pulmonary arterial hypertension. *J Am Coll Cardiol*. 2004;43(12 suppl S):13S–24S.
42. Zhang J, Patel JM, Block ER. Hypoxia-specific upregulation of calpain activity and gene expression in pulmonary artery endothelial cells. *Am J Physiol*. 1998;275(3 pt 1):L461–L468.
43. Dahal BK, et al. Role of epidermal growth factor inhibition in experimental pulmonary hypertension. *Am J Respir Crit Care Med*. 2010;181(2):158–167.
44. Amanchy R, et al. Identification of c-Src tyrosine kinase substrates in platelet–derived growth factor receptor signaling. *Mol Oncol*. 2009; 3(5–6):439–450.
45. Niapour M, Berger S. Flow cytometric measurement of calpain activity in living cells. *Cytometry A*. 2007;71(7):475–485.
46. Tan Y, Wu C, De Veyra T, Greer PA. Ubiquitous calpains promote both apoptosis and survival signals in response to different cell death stimuli. *J Biol Chem*. 2006;281(26):17689–17698.
47. Chen H, Ishii A, Wong WK, Chen LB, Lo SH. Molecular characterization of human tensin. *Biochem J*. 2000;351 pt 2:403–411.
48. Bertoli C, Copetti T, Lam EW, Demarchi F, Schneider C. Calpain small-1 modulates Akt/FoxO3A signaling and apoptosis through PP2A. *Oncogene*. 2009; 28(5):721–733.
49. Kuwano K. PTEN as a new agent in the fight against fibrogenesis. *Am J Respir Crit Care Med*. 2006; 173(1):5–6.
50. Abe M, Oda N, Sato Y. Cell-associated activation of latent transforming growth factor-beta by calpain. *J Cell Physiol*. 1998;174(2):186–193.
51. Chen YG. Endocytic regulation of TGF-beta signaling. *Cell Res*. 2009;19(1):58–70.
52. Caver TE, O'Sullivan FX, Gold LI, Gresham HD. Intracellular demonstration of active TGFbeta1 in B cells and plasma cells of autoimmune mice. IgG-bound TGFbeta1 suppresses neutrophil function and host defense against Staphylococcus aureus infection. *J Clin Invest*. 1996;98(11):2496–2506.
53. Hood JL, Brooks WH, Roszman TL. Differential compartmentalization of the calpain/calpastatin network with the endoplasmic reticulum and Golgi apparatus. *J Biol Chem*. 2004;279(41):43126–43135.
54. Gressner OA. Intracrine signaling mechanisms of activin A and TGF-β. *Vitam Horm*. 2011;85:59–77.
55. Duffy JY, et al. Calpain inhibition decreases endothelin-1 levels and pulmonary hypertension after cardiopulmonary bypass with deep hypothermic circulatory arrest. *Crit Care Med*. 2005;33(3):623–628.
56. Tabata C, Tabata R, Nakano T. The calpain inhibitor calpeptin prevents bleomycin-induced pulmonary fibrosis in mice. *Clin Exp Immunol*. 2010; 162(3):560–567.
57. Cui Z, et al. Involvement of calpain-calpastatin in cigarette smoke-induced inhibition of lung endothelial NOS. *Am J Respir Cell Mol Biol*. 2005; 33(5):513–520.
58. Youn JY, Wang T, Cai H. An ezrin/calpain/PI3K/AMPK/eNOSs1179 signaling cascade mediating VEGF-dependent endothelial nitric oxide production. *Circ Res*. 2009;104(1):50–59.
59. Su Y, Block ER. Role of calpain in hypoxic inhibition of nitric oxide synthase activity in pulmonary endothelial cells. *Am J Physiol Lung Cell Mol Physiol*. 2000;278(6):L1204–L1212.
60. Arthur JS, Elce JS, Hegadorn C, Williams K, Greer PA. Disruption of the murine calpain small subunit gene, Capn4: calpain is essential for embryonic development but not for cell growth and division. *Mol Cell Biol*. 2000;20(12):4474–4481.
61. Tan Y, Dourdin N, Wu C, De V T, Elce JS, Greer PA. Conditional disruption of ubiquitous calpains in the mouse. *Genesis*. 2006;44(6):297–303.
62. Wang Y, et al. TGF-beta activity protects against inflammatory aortic aneurysm progression and complications in angiotensin II-infused mice. *J Clin Invest*. 2010;120(2):422–432.
63. Wei W, et al. Biphasic effects of selective inhibition of transforming growth factor beta1 activin receptor-like kinase on LPS-induced lung injury. *Shock*. 2010;33(2):218–224.
64. Wang CH, et al. Protective effect of MDL28170 against thioacetamide-induced acute liver failure in mice. *J Biomed Sci*. 2004;11(5):571–578.
65. De MA, Shi Y, Kumar NM, Bassnett S. Calpain expression and activity during lens fiber cell differentiation. *J Biol Chem*. 2009;284(20):13542–13550.
66. Glantz SB, Cianci CD, Iyer R, Pradhan D, Wang KK, Morrow JS. Sequential degradation of alphaII and betaII spectrin by calpain in glutamate or maitotoxin-stimulated cells. *Biochemistry*. 2007;46(2):502–513.
67. Yoshida K, et al. Reperfusion of rat heart after brief ischemia induces proteolysis of calspectin (nonerythroid spectrin or fodrin) by calpain. *Circ Res*. 1995; 77(3):603–610.
68. Bi X, Chang V, Siman R, Tocco G, Baudry M. Regional distribution and time–course of calpain activation following kainate–induced seizure activity in adult rat brain. *Brain Res*. 1996;726(1–2):98–108.
69. Crawford SE, et al. Thrombospondin-1 is a major activator of TGF-beta1 in vivo. *Cell*. 1998; 93(7):1159–1170.
70. Colombel M, et al. Androgens repress the expression of the angiogenesis inhibitor thrombospondin-1 in normal and neoplastic prostate. *Cancer Res*. 2005;65(1):300–308.
71. Dasgupta S, Bhattacharya-Chatterjee M, O'Malley BW Jr, Chatterjee SK. Tumor metastasis in an orthotopic murine model of head and neck cancer: possible role of TGF-beta 1 secreted by the tumor cells. *J Cell Biochem*. 2006;97(5):1036–1051.
72. Dong Y, et al. Calpain inhibitor MDL28170 modulates Abeta formation by inhibiting the formation of intermediate Abeta46 and protecting Abeta from degradation. *FASEB J*. 2006;20(2):331–333.
73. Su Y, Cui Z, Li Z, Block ER. Calpain-2 regulation of VEGF-mediated angiogenesis. *FASEB J*. 2006; 20(9):1443–1451.
74. Walton KL, et al. Two distinct regions of latency-associated peptide coordinate stability of the latent transforming growth factor-beta1 complex. *J Biol Chem*. 2010;285(22):17029–17037.
75. Su Y, Cao W, Han Z, Block ER. Cigarette smoke extract inhibits angiogenesis of pulmonary artery endothelial cells: the role of calpain. *Am J Physiol Lung Cell Mol Physiol*. 2004;287(4):L794–L800.